Title: The CAP1/Prss8 catalytic triad is not involved in PAR2 activation and protease nexin-1 (PN-1) inhibition.
Authors: Crisante G, Battista L, Iwaszkiewicz J, Nesca V, Mérillat AM, Sergi C, Zoete V, Frateschi S, Hummler E
Journal: FASEB journal : official publication of the Federation of American Societies for Experimental Biology
Year: 2014 Nov
Volume: 28
Issue: 11
Pages: 4792-805
DOI: 10.1096/fj.14-253781

The CAP1/Prss8 Catalytic Triad is not Involved in PAR2 Activation and Protease Nexin-1 (PN-1) inhibition

Giovanna Crisante[1], Laura Battista[1], Justyna Iwaszkiewicz[2], Valeria Nesca[1,3], Anne-Marie Merillat[1], Chloé Sergi[1], Vincent Zoete[2], Simona Frateschi[1]* & Edith Hummler[1]*.

[1]Department of Pharmacology and Toxicology; [2]Swiss Institute of Bioinformatics, University of Lausanne, Lausanne, Switzerland.

*equally contributed (equally corresponding authors)

Simona Frateschi,

Simona.Frateschi@unil.ch

or

Edith Hummler,

Edith.Hummler@unil.ch

Department of Pharmacology & Toxicology

Rue du Bugnon 27, CH-1005, Lausanne, Switzerland

Tel. +41/21-692 5357

Fax. +41/21-692 5355

Present address:

[3]Department of Fundamental Neurosciences, University of Lausanne, Lausanne, Switzerland.

Running head: Non-enzymatic effects of prostasin

Non-standard abbreviations

CAP1/Prss8: channel-activating protease-1, protease serine S1 family member 8, prostasin

ENaC: epithelial sodium channel

HDS: histidine, aspartate and serine

IL: interleukin

K14: keratin 14

MMP9: matrix-remodeling enzyme matrix metalloproteinase 9

nexin-1: protease nexin-1, serpinE2, PN-1, glia-derived nexin

PAR2: protease-activated receptor 2, coagulation factor II (thrombin) receptor-like 1, F2RL1

PCR: polymerase chain reaction

RCL: reactive center loop

Serpins: serine protease inhibitors

tg: transgenic

TSLP: thymic stromal lymphopoietin

wt: wild-type

Abstract

Serine proteases, serine protease inhibitors, and protease-activated receptors (PARs) are responsible of several human skin disorders characterized by impaired epidermal permeability barrier function, desquamation and inflammation. In this study we addressed the consequences of a catalytically dead serine protease on epidermal homeostasis, the activation of the protease-activated receptor 2 (PAR2) and the inhibition by the serine protease inhibitor nexin-1. We show that the catalytically inactive serine protease CAP1/Prss8 retained the ability to induce skin disorders when ectopically expressed in the mouse as well as its catalytically active counterpart (75%, n=81). Moreover, this phenotype is completely normalized in a PAR2-null background, indicating that the effects mediated by the catalytically inactive CAP1/Prss8 depend on PAR2 (95%, n=131). Finally, we demonstrate that nexin-1 displayed analogous inhibitory capacity on both wild-type and inactive mutant CAP1/Prss8 *in vitro* and *in vivo* (64% n=151 versus 89% n=109, respectively) indicating that the catalytic site of CAP1/Prss8 is dispensable for nexin-1 inhibition. Our results demonstrate a novel inhibitory interaction between CAP1/Prss8 and nexin-1 opening the search for specific CAP1/Prss8 antagonists that are independent from its catalytic activity.

Key words

Serine protease, prostasin, enzymatic activity

Introduction

Serine proteases are enzymes involved in the regulation of many biological processes, and are named as such for the nucleophilic serine residue at the active site. They cleave peptide bonds by their catalytic triad of histidine, aspartate and serine (1, 2) and besides being degrading enzymes they regulate downstream signaling pathways as those triggered by protease-activated receptors (PARs) (3). Different specific inhibitors control their activities, and this accurate balance is altered in genetic defects or by exogenous influences (4). CAP1/Prss8 is a membrane-anchored serine protease expressed in the epithelium of several organs such as the skin, colon, lung and kidney (5-8) and it can be released in the extracellular space by the action of phospholipase C (9, 10). The catalytic triad of human and mouse CAP1/Prss8 was identified as His85, Asp134 and Ser238 according to multiple sequence alignment with other known serine proteases (11). CAP1/Prss8 was the first of several membrane-bound serine proteases, like CAP2/TMPRSS4 and CAP3/matriptase found to activate the epithelial sodium channel (ENaC) in *Xenopus* oocytes (12, 13) and in rodents (8, 14, 15). An intact catalytic triad is required for activation of ENaC by CAP2/TMPRSS4 and CAP3/matriptase, but not by CAP1/Prss8 (16). Conditional removal of CAP1/Prss8 in mouse skin induces postnatal death (5), whereas increased expression of CAP1/Prss8 impairs survival and leads to disease demonstrating that balanced CAP1/Prss8 expression is required for skin homeostasis (17). Moreover, absence of the protease activated receptor 2 (PAR2) completely restores the defects caused by CAP1/Prss8 overexpression in the skin revealing PAR2 as crucial mediator of CAP1/Prss8 signaling (17).

The secreted form of CAP1/Prss8 can bind the serine protease inhibitor nexin-1 also known as serpinE2, PN-1, and glia-derived nexin (9, 18). In addition, CAP1/Prss8-induced ENaC-mediated sodium currents can be inhibited by nexin-1 in the *Xenopus* oocytes (19). Nexin-1 belongs to the serpin family of serine protease inhibitors considered to exert an inhibitory

action by forming covalent and therefore irreversible complexes through their reactive center loop with the serine of the catalytic triad of their substrates (20) (21). Nexin-1 is the most abundant potent endogenous brain thrombin inhibitor (22), and mice deficient for the gene encoding nexin-1 do no present any obvious skin phenotype (23). Nexin-1 is also expressed in the skin in the mesenchymal population of the hair follicle where it regulates the plasticity of dermal cells (24, 25).

In the present study we aimed to analyze the consequences of H85A, D134A and S238A (namely HDS-A) CAP1/Prss8 mutations for skin physiology when over-expressed, and the impact on nexin-1 inhibition and PAR2 activation. *K14-CAP1/Prss8*$^{HDS\text{-}A}$ transgenic animals mimic the phenotype of mice with increased expression of non-mutant CAP1/Prss8 in the skin, and this phenotype could be completely restored in a PAR2-null background, indicating that the enzymatically inactive CAP1/Prss8$^{HDS\text{-}A}$ mutant is still able to activate PAR2. Furthermore, nexin-1 presented equivalent inhibitory capacity on each active and inactive mutant CAP1/Prss8 *in vitro* and *in vivo*, showing that the catalytic site of CAP1/Prss8 is dispensable for nexin-1 inhibition.

Materials and methods

Mice and measurements of scratching behavior. The H85A, D134A and S238A mutations were all inserted into the mouse *CAP1/Prss8* coding sequence (Genbank g.i. 19111159) and introduced into the pBHR2(SmaI) vector (17) to generate the *K14-CAP1/Prss8*$^{HDS\text{-}A}$ transgenic mice. The *K14-CAP1/Prss8* and *K14-CAP1/Prss8*$^{HDS\text{-}A}$ transgenes could be differentiated one from another by PCR, because of 50 base pairs difference at level of the DNA construct (Fig. 1A and Supplementary Fig. 1C). *K14-nexin-1* transgenic animals were generated by cloning the mouse *nexin-1* cDNA (Genbank g.i. 229093415) into the same pBHR2(SmaI) vector. Vector sequences were removed and the linearized constructs were microinjected into B6D2F1 hybrid zygotes. Transgenic lines were maintained in the hemizygous state and compared to non-transgenic littermates hereafter named wild-type mice. Transgenic mice were genotyped by PCR and Southern blot analysis of genomic DNA extracted from tail biopsies (17, 26). Experimental procedures and animal maintenance followed federal guidelines and were approved by local authorities. For assessing the scratching behavior, simultaneous experiments were conducted on five mice in the absence of investigators. Mice were not in contact with each other during the experiment. The mice were videotaped for 20 min for later quantification of scratching behavior. One scratch was considered as lifting of a limb towards the body with subsequent replacement of the limb on the bedding. The scratching was quantified in a 10 min time period and expressed as percentage of total time, as previously described (17).

TEWL measurements. The rate of trans-epidermal water loss (TEWL) was measured using a Tewameater TM210 (Courage and Khazaka, Köln, Germany) from the ventral skin of pre-shaved, anesthetized two week-old transgenic and littermate controls. Four independent measurements were performed per animal. The mean ± SEM results are given, as previously described (17).

Semiquantitative and quantitative RT-PCR. Skin was homogenized using Tissue Lyzer (Qiagen, Valencia, CA) and RNA was extracted with the Qiagen RNeasy Mini kit (Basel, Switzerland) following the manufacturer instructions. A volume of 1 µg of RNA was reverse transcribed using PrimeScript^{TM} reagent Kit (Takara bio inc.). Real-time PCR were performed by TaqMan PCR or Sybergreen using Applied Biosystems 7500. Each measurement was performed in triplicate. Quantification of fluorescence was normalized to β-actin. Primer sequences were previously published in (17). The endogenous *CAP1/Prss8* expression was assessed by endogenous-specific primers (only_endog_CAP1_S 5' CCTGGGATTCCTCACTCTGA 3' and only_endog_CAP1_A 5' CGAGAAGGAGCAGAATGGTC3'). The *K14-nexin-1* transgene expression was assessed by PN_1_F 5' TTCCGCTCAGGGTCTACCAG 3', PN_1_probe 5' GCATGCTGATCGCCCTGCCA 3' and PN_1_R 5' TGAGGGATGATGGCAGACAG 3' primers.

Immunofluorescence, histology and Western blot. Skin was embedded into paraffin. Slides were incubated in xylene for at least 4 hours and rinsed with decreasing concentrations of ethanol. Antigen retrieval was performed for 10 min in TEG buffer. Slides were washed in 50 mM NH_4Cl in PBS for 30 min and blocked by 1% BSA, 0.2% gelatine, 0.05% Saponin in PBS at room temperature for 10 min, three times. Primary antibody was diluted in 0.1% BSA, 0.3% Triton X-100 in PBS, overnight at 4 °C. Antibodies against keratin-14, keratin-1, keratin-6, involucrin, loricrin and filaggrin were purchased from Covance and diluted 1:1,000 or 1:4,000 (keratin-14). Affinity-purified CAP1/Prss8 rabbit anti-mouse antiserum (27) was diluted 1:200. This antibody was validated on knock out mouse tissues (5) and can recognize mutant and wild-type CAP1/Prss8 (16). Slides were rinsed three times for 10 min in PBS containing 0.1% BSA, 0.2% gelatine and 0.05% saponin at room temperature and the secondary antibody (Alexa Fluor 488, diluted 1:5,000; Invitrogen, Grand Island, NY) was

diluted in 0.1% BSA, 0.3% Triton X-100 in PBS. Nuclei were counterstained with 4,6-diamidino-2-phenylindole (DAPI) 0.2 μg/ml in mounting media (Dako Schweiz AG). Staining was visualized using an LSM confocal microscope (LSM 510 Meta, Carl Zeiss MicroImaging Inc., Jena, Germany).

For H&E staining, paraffin was removed and the slides were rehydrated 2 times in xylol for 5 minutes, 2 times in 100% ethanol for 1 minute, in 95% ethanol for 1 minute, and finally rinsed with tap water. Slides were incubated in staining glychemalun solution (0.013 mol/L Hematein, Gurr #34036; 0.3133 mol/L potassium alum, Merck #1047; 30% glycerol; 1% acetic acid, Merck #1.00063) for 4 minutes, tap water, 1% acid alcohol for 3 seconds, tap water, water for 15 seconds plus a few drops of NH3, tap water, 0.2% erythrosine solution (0.0023 mol/L erythrosin, Merck #15936; 0.1% formaldehyde, Merck #4003) for 30 seconds, and finally rinsed with tap water. Slides were then dehydrated by following steps from 70% ethanol to xylol and mounted (Eukitt, Hatfield, PA). Pictures were taken using an Axion HRC (Carl Zeiss MicroImaging Inc.). Western blot from skin samples were performed as previously described (17).

Construct preparation. The H85A D134A S238A (HDS-A), E247A (E-A), and E247A I249A W250A Y251A (EIWY-A) mutations were inserted into the mouse *CAP1/Prss8* coding sequence (GenBank gi 19111159) by standard PCR-directed mutagenesis, and the resulting mutants were named CAP1/Prss8^{HDS-A}, CAP1/Prss8^{E-A}, and CAP1/Prss8^{EIWY-A}, respectively. Wild-type and mutant CAP1/Prss8 constructs (CAP1/Prss8^{HDS-A}, CAP1/Prss8^{E-A}, and CAP1/Prss8^{EIWY-A}) were introduced in the pSDeasy expression vector (14) and pRK5 vector (28) for *in vitro* transcription and HEK-293 cell transfection, respectively. The mouse *nexin-1* coding sequence (Genbank gi 229093415) and the mouse *PAR2* coding sequence (Genbank gi 142349952) were also introduced into the pSDeasy and pRK5 expression vectors to generate nexin-1 and PAR2 constructs, respectively. The Flag-tag (DYKDDDDK) was

inserted between amino acid P211 and E212 in all CAP1/Prss8 constructs, and at the N terminus of nexin-1. The HA-tag (YPYDVPDYA) was added at the C terminus of PAR2.

***Xenopus* oocyte injections and electrophysiologic measurements.** The SP6 RNA polymerase (Promega, Madison, WI) was used for cRNA synthesis. Expression studies performed in *X. laevis* oocytes (obtained from African Xenopus Facility, Noordhoek, South Africa) in stage V/VI have been previously described (14, 29).

HEK-293 cell transfections and co-immunoprecipitation experiments. HEK-293 cells were cultured in Dulbecco's modified Eagle's medium (DMEM) supplemented with 10% fetal bovine serum and 100 µg/mL gentamicin and transfected at 50% to 60% confluence in 100-mm dishes using the calcium-phosphate method. After transfection, cells were grown for 48 hours in DMEM supplemented with 10% fetal bovine serum before harvesting. The total amount of transfected DNA was 12 µg per 100-mm dish. Cells were lysed using 1 mL of lysis buffer 20 mM Tris-HCl pH 7.4; 150 mM NaCl; 1% Triton X-100; 2µg/mL Pepstatin A, 5 µg/mL Aprotinin; 4 µg/mL Leupeptin; 1 mM PMSF per 100-mm dish. Lysates were incubated 30 min at 4°C on a rotating wheel. The solubilized material was centrifuged 15000 rpm for 15 min at 4°C. Supernatants were incubated for 2 h at 4°C with monoclonal anti-Flag M2 beads (Sigma, Switzerland) or with monoclonal anti-HA beads (anti-HA-Agarose, antibody produced in mouse, Sigma, Switzerland) to immunoprecipitate over-expressed Flag-tagged and HA-tagged proteins. Following a brief centrifugation at 4°C on a bench-top centrifuge, the pelleted beads were washed with lysis buffer three times during 10 min with on a rotating wheel at 4°C. Proteins were eluted in SDS-PAGE sample buffer following boiling for 5' at 95° C. Proteins were analyzed by Western blotting using a Flag-tagged and a HA-tagged antibody (Monoclonal Anti-HA antibody produced in mouse clone HA-7, ascites fluid, Sigma, Switzerland) to detect immunoprecipitates and/or cells extracts, and using a mouse anti-mouse nexin-1 and/or an anti-mouse CAP1/Prss8 (27) antibody to detect co-

immunoprecipitated proteins. The nexin-1 antibody was kindly provided by Denis Monard (Friedrich Miescher Institute For Biomedical Research, Basel, Switzerland). Signals were revealed using anti-mouse IgG from goat (1:5000, GE Healthcare, Glattbrugg, Switzerland) as secondary antibody and ECL^{TM} Western Blotting Detection Reagents (GE Healthcare).

Mass spectrometry. HEK-293 cells were co-transfected with either wild-type or catalytically mutant CAP1/Prss8 (CAP1/Prss8^{HDS-A}) and nexin-1-Flag. Proteins were incubated with beads anti-Flag and separated on 5-15 % SDS-PAGE gel and processed with Comassie blue. The 75-kDa and the 37-43-kDa band detected in both conditions were cut and digested with sequencing-grade trypsin (Promega) as described (30),(31). Data-dependent LC-MS/MS analysis of extracted peptide mixtures after digestion was carried out on a hybrid linear trap LTQ-Orbitrap mass spectrometer (Thermo Fisher Scientific) interfaced via a TriVersa Nanomate (Advion Biosciences) to an Agilent 1100 nano HPLC system (Agilent Technologies). Peptides were separated on a ZORBAX 300SB C18 (75 μm ID x 150 mm, 3.5 μm) capillary column (Agilent Technologies) along a 90 min gradient from 5 to 85 % acetonitrile in 0.1% formic acid at a flow rate of 300 nl/min. From raw files, MS/MS spectra were de-isotoped and exported as mgf files (Mascot Generic File, text format) using MascotDistiller 2.1.1 (Matrix Science, London, UK). MS/MS spectra samples were searched using Mascot (Matrix Science, London, UK; version 2.2.0) against the UNIPROT database, (SWISSPROT + TrEMBL, www.expasy.org) restricted to mammalian taxonomy. The database release used was 2011_03 of March 8, 2011 (372436 sequences after taxonomy filter) with trypsin specificity, fragment ion mass tolerance of 0.5 Da and parent ion tolerance of 10 ppm. The iodoacetamide derivative of cysteine was specified as a fixed modification, and oxidation of methionine as a variable modification. Scaffold (version Scaffold-01_06_03, Proteome Software Inc.) was used to validate MS/MS based peptide and protein identifications. Peptide identifications were accepted if they could be established at greater

than 95.0% probability as specified by the Peptide Prophet algorithm (32). Protein identifications were accepted if they could be established at greater than 99.0% probability and contained at least 2 identified peptides. Protein probabilities were assigned by the Protein Prophet algorithm (33). Proteins that contained similar peptides and could not be differentiated based on MS/MS analysis alone were grouped to satisfy the principles of parsimony. Protein lists for further analysis were exported with Scaffold. Differentially detected proteins (absent in one sample or with varying numbers of spectra) were manually validated.

Homology modeling and docking analyses. Mouse CAP1/Prss8 and nexin-1 three-dimensional structures were modeled using the crystal structure-based homology model of human CAP1/Prss8 (34) and Plasminogen Activator Inhibitor-1 (PAI-1) in its latent form (35) as templates. The sequence identity between the mouse and human CAP1/Prss8 is 77.5%. The sequence identity between nexin-1 and PAI-1 is 41.5%. The recently crystallized human nexin-1 structure (36) could not be used as a template because the protein was crystallized in the active conformation. The structure-based modeling and alignments were performed with Modeller 9v5 software (37). Based on pairwise alignments with the template structures, 100 models were produced, and the best models were chosen according to ANOLEA score (38). Predictions of the interaction interface between nexin-1 and CAP1/Prss8 were carried out with the WHISCY server (39). ZDOCK(40) and HADDOCK (41) protein-protein docking programs were employed to predict nexin-1 and CAP1/Prss8 interaction mode. The residues previously predicted by WHISCY server were given as the plausible interaction centers during the docking procedures. Both programs proposed very similar complex structures as the top-scored prediction. The nexin-1 / CAP1/Prss8 complex conformation predicted by HADDOCK was used as a starting point for a molecular dynamics simulation. The 10 ns-long molecular dynamics simulation was performed using the Gromacs and the CHARMM22

programs (42),(43). The 250 nexin-1/ CAP1/Prss8 structures derived from molecular dynamics trajectory were used to calculate the free energy of interaction with the MM-GBSA method (44). The residues contributing the most to the interaction and located in the center of the interaction interface, were selected for mutagenesis, and their impact on protein stability was assessed by computational alanine scanning using the FoldX program (45).

Statistical analysis. Phenotype frequencies were analyzed by chi-square test. All data are expressed as means ± s.e.m. Individual groups were compared using one-way ANOVA test, followed by the Wilcoxon Mann-Whitney test for individual comparisons. Bonferroni correction for planned multiple comparisons was included. Statistical analyses were performed using GraphPad Prism Version 6.01. A level of $p < 0.05$ was considered statistically significant for all comparisons; * $p < 0.05$, ** $p < 0.01$, *** $p < 0.001$, ns non-significant.

Results

Transgenic expression of mutant CAP1/Prss8^{HDS-A} in the skin causes disease

Transgenic over-expression of the serine protease CAP1/Prss8 in the epidermis severely compromises skin function leading to ichthyosis, hyperplasia, inflammation, and increased itch (17). To investigate the importance of the putative H85, D134 and S238 CAP1/Prss8 catalytic triad in determining the observed phenotype we targeted the expression of the catalytically inactive mutant CAP1/Prss8 in which H85, D134 and S238 were mutated into alanine (HDS-A) (16) to the keratin-14-expressing cells using *K14-CAP1/Prss8^{HDS-A}* transgenic mice (Fig. 1A, Supplementary Fig. 1A, B and C; and Table 1). The *K14-CAP1/Prss8^{HDS-A}* transgenic mice expressed the transgene in the skin as demonstrated by real-time PCR and immunofluorescence, and endogenous *CAP1/Prss8* mRNA levels were not affected by the expression of the *CAP1/Prss8^{HDS-A}* transgene (Fig. 1B and C). *K14-CAP1/Prss8^{HDS-A}* animals presented with scaly skin (ichthyosis) and epidermal hyperplasia (acanthosis, Fig. 1D) as *K14-CAP1/Prss8* animals that over-expressed the wild-type form of CAP1/Prss8 in the skin (17). Furthermore, keratin-1, loricrin, filaggrin and involucrin appeared to be more widespread within the epidermis of *K14-CAP1/Prss8^{HDS-A}* mice compared to wild-types, and expression levels tended to increase (Fig. 1E and Supplementary Fig. 1D). Keratin-14 was detected in all nucleated epidermal cell layers, and keratin-6 was also visible in interfollicular keratinocytes (Fig. 1E). Although we did not record differences in body weight among 2 week-old wild-type and transgenic animals (wt, n=14, 6.9±0.22 versus tg, n=18, 6.7±0.19 grams, p=0.239), the TEWL of *K14-CAP1/Prss8^{HDS-A}* mice was significantly higher compared to controls (Fig. 1F). The cytokines interleukin-1α (IL-1α), interleukin 1β (IL-1β), thymic stromal lymphopoietin (TSLP) and the extracellular matrix-remodeling enzyme matrix metalloproteinase-9 (MMP9) were highly up-regulated in *K14-CAP1/Prss8^{HDS-A}* mice relative to littermate controls (Fig. 1G). Finally,

scratching behavior in *K14-CAP1/Prss8*$^{HDS-A}$ animals was also significantly increased (Fig. 1 H). These data show that the expression of the *K14-CAP1/Prss8* and *K14-CAP1/Prss8*$^{HDS-A}$ transgenes results in a comparable phenotype, and highly suggest that the ability of CAP1/Prss8 to induce pathology in the skin when misexpressed does not depend on its catalytic triad.

CAP1/Prss8 interacts with PAR2 *in vitro* despite the HDS-A mutations

To investigate whether the catalytic triad of CAP1/Prss8 is involved in the interaction of CAP1/Prss8 with PAR2, we performed co-immunoprecipitation studies in HEK-293 cells. We co-transfected the cells with CAP1/Prss8 wild-type or CAP1/Prss8^{HDS-A} and PAR2, and found that PAR2 can physically interact with both CAP1/Prss8 and CAP1/Prss8^{HDS-A} (Fig. 2A and B). These data suggest that the intact CAP1/Prss8 catalytic triad is not required for the interaction of CAP1/Prss8 with PAR2.

PAR2 deficiency rescues *K14-CAP1/Prss8*$^{HDS-A}$-induced skin defects

To experimentally test whether the phenotype in *K14-CAP1/Prss8*$^{HDS-A}$ transgenic animals is due to enhanced PAR2 activation we crossed *K14-CAP1/Prss8*$^{HDS-A}$ transgenic mice with animals deficient in PAR2 (*PAR2* -/-) (46).

Compared to wild-type littermates the *K14-CAP1/Prss8*$^{HDS-A}$ mice being wild-type, heterozygous mutant or homozygous mutant for *PAR2* expressed higher levels of total (endogenous plus transgene-driven) *CAP1/Prss8* transcripts (Fig. 3A), and reduced or absent *PAR2* transcription in the *PAR2* +/- and *PAR2* -/- background, respectively (Fig. 3B). *K14-CAP1/Prss8*$^{HDS-A}$ mice harboring either the wild-type (*PAR2* +/+) or the heterozygous mutant allele for PAR2 (*PAR2* +/-) displayed scaly skin with epidermal hyperplasia. In contrast, scaling and epidermal hyperplasia were never observed in *K14-CAP1/Prss8*$^{HDS-A}$ mice that

were homozygous mutant for PAR2 (*PAR2 -/-*, Fig. 3C, D and Table 2). The rescue was also functionally evident, as *K14-CAP1/Prss8^{HDS-A}; PAR2 -/-* mice exhibited a TEWL in the same range as wild-type controls, but significantly different from that of *K14-CAP1/Prss8^{HDS-A};PAR2 +/+* littermates (Fig. 3E). Moreover, with the exception of *IL-1α* the mRNA transcript expression levels of inflammatory markers *IL-1β, TSLP and MMP9* were comparable to control levels in *K14-CAP1/Prss8^{HDS-A}; PAR2 -/-* animals (Fig 3F). Finally, PAR2 absence restored the scratching behavior in these animals to control levels (Fig 3G). Thus, absence of PAR2 completely rescued hyperplasia, barrier dysfunction, inflammation, ichthyosis and itch caused by transgenic *K14-CAP1/Prss8^{HDS-A}* expression in the skin indicating that the catalytically inactive CAP1/Prss8^{HDS-A} is still able to activate PAR2.

Nexin-1 inhibits and interacts with CAP1/Prss8 wild-type and CAP1/Prss8^{HDS-A} *in vitro*

The serine protease inhibitor nexin-1 has been identified as a CAP1/Prss8-binding protein (18). To study the inhibition of CAP1/Prss8 by nexin-1 we performed co-immunoprecipitation and electrophysiological studies to investigate the ability of CAP1/Prss8 and nexin-1 to interact. We transfected HEK293 cells with Flag-tagged CAP1/Prss8 with or without the mutant catalytic site (CAP1/Prss8^{HDS-A}), and/or with nexin-1. Using anti-Flag beads we immunoprecipitated the CAP1/Prss8 wild-type and CAP1/Prss8^{HDS-A} mutant proteins, and with the anti-nexin-1 antibody we found that nexin-1 co-immunoprecipitates with each CAP1/Prss8 wild-type and CAP1/Prss8^{HDS-A} (Fig. 4A), and can also form a complex of 75 kDa (Fig. 4A open arrow, and Supplementary Table 1). We then used the two-electrode voltage-clamp method in *Xenopus* oocytes to study the effect of nexin-1 on CAP1/Prss8-induced ENaC activation. We observed that CAP1/Prss8 wild-type and CAP1/Prss8^{HDS-A} mutant are both able to activate ENaC, and co-expression of nexin-1 significantly decreased both the CAP1/Prss8 wild-type and CAP1/Prss8^{HDS-A}-activated

sodium currents (Fig. 4B). We could therefore clearly demonstrate that nexin-1 interacts with and inhibits CAP1/Prss8 despite the inactivation of its catalytic site.

Consequently, to show that such inhibition is accomplished by protein-protein interaction regardless of the CAP1/Prss8 catalytic site, we built a homology model of mouse CAP1/Prss8 and nexin-1 using as templates the crystal structure-based models of human CAP1/Prss8 and plasminogen activator inhibitor-1, respectively, and performed *in silico* docking analyses using ZDOCK and HADDOCK programs, to predict the preferred orientation of CAP1/Prss8 to nexin-1 when bound to form a stable complex (Fig. 4C and D). Among top-scored prediction we found similar complex structures in case of both methods. We found that the buried surface area is over 2000 $Å^2$. The CAP1/Prss8 region involved in the interaction comprises the amino acid residues 241-255 in which Glu 247 makes hydrogen bond with the Lys 396 residue in nexin-1. Conversely, the CAP1/Prss8 catalytic triad is not involved in the interaction. The nexin-1 interacting surface is at the C-terminal face of the protein (Fig. 4C) and close to the recently described thrombin binding site (36). We thus decided to mutate Glu 247 into Alanine in CAP1/Prss8 (CAP1/$Prss8^{E\text{-}A}$) and looked at CAP1/Prss8 and nexin-1 interactions. CAP1/$Prss8^{E\text{-}A}$ and nexin-1 are still able to co-immunoprecipitate, but their interaction is reduced (Fig. 4E). Altogether, these results strongly suggest that the CAP1/Prss8 catalytic triad is not involved in nexin-1 interaction. They also indicate that the classical involvement of the reactive center loop of the serpin is not required for this interaction.

Epidermal nexin-1 overexpression blunts the pathological effects caused by *K14-CAP1/Prss8* and *K14-CAP1/*$Prss8^{HDS\text{-}A}$ transgenes

We then asked whether nexin-1 can inhibit CAP1/Prss8 in living organisms, and used the skin as a system of investigation *in vivo* to analyze whether balanced expression of nexin-1 and CAP1/Prss8 is necessary for skin physiology. We thus generated *K14-nexin-1* transgenic mice

by placing the mouse *nexin-1* coding sequence under the control of the human *keratin-14* promoter using the same basic construct as that of *K14-CAP1/Prss8* and *K14-CAP1/Prss8*$^{HDS-A}$ transgenic animals (Fig. 5A and Supplementary Fig. 2A, B and C). *K14-nexin-1* transgenic animals presented higher levels of total (transgenic plus endogenous) *nexin-1* mRNA and protein in the skin compared to control littermates (Fig. 5B and C). Nevertheless, they looked indistinguishable from their wild-type littermates in terms of skin architecture, histology and water loss (Fig. 5D and E) showing that increased expression of nexin-1 in the skin does not affect skin physiology.

To evaluate the capability of nexin-1 to inhibit CAP1/Prss8 in our *in vivo* model and to investigate whether this inhibition is accomplished through the CAP1/Prss8 catalytic site as proposed for serpins (20) we crossed *K14-CAP1/Prss8* and *K14-CAP1/Prss8*$^{HDS-A}$ mice with *K14-nexin-1* transgenic animals (Table 3). Compared to wild-type littermates the resulting *K14-CAP1/Prss8; K14-nexin-1* and *K14-CAP1/Prss8*$^{HDS-A}$*; K14-nexin-1* double-transgenic mice expressed higher levels of total (endogenous plus transgene-driven) *CAP1/Prss8* and *nexin-1* mRNA transcripts, as well as single transgenic animals (Fig. 6A and B, and Supplementary Fig. 3A and B). As previously reported (17), mice carrying the *K14-CAP1/Prss8* transgene and originating from two different founders (termed line 1 and 2) displayed scaly skin with epidermal hyperplasia with 100% penetrance. In contrast, scaling or epidermal hyperplasia was not observed in 96% of *K14-CAP1/Prss8* transgenic mice from line 1 and in 64% of *K14-CAP1/Prss8* transgenic mice from line 2 while carrying the *K14-nexin-1* transgene (Fig. 6C and D, Supplementary Fig. 3C and D, and Table 3). Surprisingly, the presence of the *K14-nexin-1* transgene prevented the scaly skin and epidermal hyperplasia in 89% of *K14-CAP1/Prss8*$^{HDS-A}$*; K14-nexin-1* double-transgenic mice (Fig. 6C and D, and Table 3). A small percentage of double transgenic animals (4% for *K14-CAP1/Prss8; K14-*

nexin-1 from Line 1; 36% for *K14-CAP1/Prss8; K14-nexin-1* from Line 2; and 11% for *K14-CAP1/Prss8^{HDS-A}; K14-nexin-1*; Table 3) still presented ichthyosis.

Mice transgenic for *K14-CAP1/Prss8* also manifested a significant reduction in body weight accompanied by a significant increase in TEWL. Those defects were completely abolished in *K14-CAP1/Prss8; K14-nexin-1* double-transgenic animals (Fig. 6E) and TEWL was reduced to control levels in *K14-CAP1/Prss8; K14-nexin-1* and *K14-CAP1/Prss8^{HDS-A}; K14-nexin-1* double-transgenic mice (Fig. 6F, G and Supplementary Fig. 3F). As observed for skin appearance, histology and TEWL, over-expression of *IL-1α, IL-1β, TSLP* and *MMP9* was also completely abrogated by combined over-expression of *K14-CAP1/Prss8; K14-nexin-1* and *K14-CAP1/Prss8^{HDS-A}; K14-nexin-1* transgenes (Fig. 7A, B and Supplementary Fig. 3G). Taken together, these data indicate that nexin-1 inhibits CAP1/Prss8 despite the mutation of its catalytic triad suggesting a novel mechanism of inhibitory interaction that does not require the classical involvement of the reactive center loop of the serpin.

Discussion

The biological function of CAP1/Prss8, and its potential effectors or inhibitors are still largely unknown. Mice that constitutively lack CAP1/Prss8 die because of placental insufficiency (47). Though, embryos lacking CAP1/Prss8 specifically in the skin develop normally, presenting postnatal mortality caused by epidermal dehydration, and displaying impaired tight junction functionality and altered profilaggrin processing (5). On the other hand, increased expression of CAP1/Prss8 in mouse skin causes severe disease that can be prevented by additional deletion of the *PAR2* gene (17). CAP1/Prss8 is also expressed in the alveolar epithelium and in the intestine, and mice lacking CAP1/Prss8 in alveolar and intestinal cells, exhibit decreased ENaC-mediated sodium current (8, 15). Moreover, two spontaneous rat and mouse CAP1/Prss8 mutants present reduced basal activity of ENaC in the distal colon (14). Thus, CAP1/Prss8 emerges as involved in various different processes that range from organ integrity to disease, and filaggrin, tight junctions, ENaC and PAR2 arise as direct or indirect CAP1/Prss8 targets *in vivo*. However, to which extent CAP1/Prss8 catalytic triad is responsible for those effects and interactions remains to be determined. Recently, we and others provided evidences for CAP1/Prss8 effects independent from its catalytic activity (16, 48). In the present study we asked first, whether the consequences of altered CAP1/Prss8 expression are independent from its catalytic site and mediated via the activation of PAR2 and, second whether nexin-1 is able to inhibit both the catalytically active and inactive CAP1/Prss8.

Indeed, over-expression of the K14-CAP1/Prss8$^{HDS\text{-}A}$ in the skin caused ichthyosis, hyperplasia and inflammation as seen in *K14-CAP1/Prss8* transgenic animals over-expressing the wild-type form of CAP1/Prss8 (17) indicating that the catalytic triad in CAP1/Prss8 (H85, D134 and S238) is not required to induce disease. Consistent with our findings, catalytically active and inactive CAP1/Prss8 appeared biologically active *in vivo* when

overexpressed in the epidermis of transgenic mice (49) giving rise to a severe skin phenotype similar to that observed in *K14-CAP1/Prss8* and *K14-CAP1/Prss8*$^{HDS-A}$ transgenic animals. Although, we cannot exclude that both the remaining endogenous and the catalytically inactive CAP1/Prss8 transgene expression levels participate in the observed phenotype, , following recent findings strongly support our data. Only recently, Peters and coworkers generated mice homozygous mutant for the *CAP1/Prss8*^{S238A} allele that should render the protease enzymatically inactive. These mice exhibit whisker and pelage hair defects (50), although it is not reported whether the phenotype is normalized onto a *PAR2* knockout background. Furthermore, these mice resemble the *frizzy* mice carrying a point mutation in the CAP1/Prss8 gene (V170D) (14) and the *K14-CAP1/Prss8* (17) and *K14-CAP1/Prss8*$^{HDS-A}$ transgenic mice (Fig. 1D).

Several hypotheses have been advanced as to what mechanism controls PAR2 activation by CAP1/Prss8, if the activation is direct or not, and whether it is mediated by the catalytic site of CAP1/Prss8 (17, 49, 51). The close similarities between *K14-CAP1/Prss8* and *K14-CAP1/Prss8*$^{HDS-A}$ transgenic mice are due to increased PAR2 activation in both models, as PAR2 absence can prevent skin defects induced by increased expression of both CAP1/Prss8 and CAP1/Prss8^{HDS-A}. Accordingly, we found no CAP1/Prss8 cleavage consensus site on PAR2, and CAP1/Prss8 could interact and co-immunoprecipitate with PAR2 despite the CAP1/Prss8^{HDS-A} mutation, although we do not exclude the implication of additional molecules in this interaction. Other studies reported that CAP1/Prss8 can not directly activate PAR2 and that CAP1/Prss8-induced signaling is dependent on intermediate activation of the serine protease CAP3/matriptase which is in turn an activator of PAR2. CAP1/Prss8 was found exclusively in its uncleaved form in CAP3/matriptase-deficient skin, suggesting that CAP3/matriptase cleaves and activates CAP1/Prss8 in mouse epidermis (52). However, it was also recently reported that epidermal overexpression of the activation cleavage site-mutated

CAP1/Prss8 resulted in phenotypes that were indistinguishable from mice expressing wild-type CAP1/Prss8 (49), suggesting that zymogen activation of CAP1/Prss8 is not required to elicit biological response *in vivo*, and thus CAP3/matriptase activation.

Increased scratching behavior and overexpression of several cytokines such as IL-1α, IL-1β and TSLP were observed in both *K14-CAP1/Prss8* and *K14-CAP1/Prss8*$^{HDS\text{-}A}$ transgenic mice, and abolished by the absence of PAR2. TSLP expression is linked to many disease states including asthma (53), inflammatory arthritis (54), atopic dermatitis (55), eczema (56) and other allergic disorders (57), and PAR2 plays an important role in TSLP production in keratinocytes (58). TSLP is known to mediate itch (59) and to activate Langerhans cells in the epidermis and cause inflammation (57), and we previously demonstrated that hyperplasia and inflammation in the skin of CAP1/Prss8 overexpressing mice both originate in keratinocytes directly triggered by a protease signaling cascade, indicating a cell-autonomous phenotype (17). In this study we provide evidences that a possible CAP1/Prss8-PAR2-TSLP cascade might not require the catalytic activity of CAP1/Prss8.

To evaluate the ability of the serine protease inhibitor nexin-1 to negate the effects of CAP1/Prss8 overexpression *in vivo*, we ectopically expressed nexin-1 in the mouse epidermis and obtained *K14-nexin-1* transgenic mice. In contrast to CAP1/Prss8, expression of nexin-1 in keratin 14 expressing cells did not affect skin physiology and structure, suggesting that skin homeostasis is less sensitive to differential expression of serine protease inhibitors compared to serine proteases. This was also described for the serine protease inhibitor hepatocyte growth factor activator inhibitor type 1, HAI-1, and the serine protease CAP3/matriptase (60). Surprisingly, nexin-1 presented the same inhibitory capacity on both *K14-CAP1/Prss8* and *K14-CAP1/Prss8*$^{HDS\text{-}A}$ mice indicating that the catalytic triad of CAP1/Prss8 is dispensable for nexin-1 inhibition. The phenotypic variation between the different *K14-CAP1/Prss8 / K14-nexin-1* and *K14-CAP1/Prss8*$^{HDS\text{-}A}$ */ K14-nexin-1* double transgenic mouse lines may be

attributed to unbalanced expression of the CAP1/Prss8 and nexin-1 transgenes. Analogous results could be observed *in vitro*, as nexin-1 co-immunoprecipitated and inhibited both the wild-type and the mutant CAP1/Prss8^{HDS-A} protein.

Signaling triggered by enzymatically inactive nexin-1/protease complexes upon interaction with the low-density lipoprotein receptor-related protein-1 (LRP-1) has been described earlier (61). The nexin-1 epitope involved has been identified, and a corresponding peptide prevents the interaction (62). Interestingly, this type of LRP-1 mediated signaling stimulates the up-regulation of MMP-9, thus contributing to the metastatic potential of tumor cells (63). The effect on MMP-9 expression is antagonized by the peptide preventing the interaction with LRP-1. In such mechanism, the formation of covalent and irreversible complexes requires the reactive center loop of the serpin and the catalytic triad of the serine protease leading to drastic structural changes and exposure of previously hidden epitopes (64). The results presented in this communication provide a completely new and distinct perspective in considering how the homeostasis between serine proteases and serpins affects biological processes. Not only the catalytic triad is not required, but also nexin-1 is shown to still interact with such proteolytically inactive CAP1/Prss8 and the amino acid residues most probably involved are distinct from the reactive center loop. The specificity of nexin-1 in this new type of mechanism, namely the potential of other serpins or inhibitors to antagonize the catalytically inactive CAP1/Prss8 will require further investigations. It also remains to be established whether this new type of complex formation is just inhibiting CAP1/Prss8 without having additional signaling function. It is nevertheless worth stressing that this type of inhibition antagonizing PAR2 signaling can have completely opposite biological consequences than the interaction of nexin-1 with catalytically active protease triggering LRP-1 signaling, as MMP-9 is downregulated in one case and upregulated in the other (62).

The *in vivo* results presented here are based on the expression of the transgenes in the basal layer of the epidermis. This expression does not necessarily mimic the sites and the levels of expression of the players in the epidermis of the wild-type mice. Nevertheless the phenotypes demonstrate that this new type of interaction between CAP1/Prss8 and nexin-1 may have relevance *in vivo*. Finally, CAP1/Prss8 has been proposed as a target for therapeutic inhibition and mimetic peptides serving as enzymatic substrates have started to be developed (65). Indeed, molecular strategies which will be designed to inhibit non-enzymatic CAP1/Prss8 action will provide therapeutic benefits to patients suffering from skin disorders.

Acknowledgements

We thank all of the members of the Hummler Laboratory and Bernard Rossier for helpful discussions.We thank Friedrich Beermann and Denis Monard for critically reading the manuscript, and Denis Monard for for providing us with the nexin-1 antibody. We like to thank Nicole Fowler-Jaeger for excellent technical assistance with the *Xenopus* oocyte injections and measurements. We also thank Olivier Michielin for helpful discussion on bioinformatic approaches. We are grateful to the Facilities of the Mouse Pathology, the Protein Analysis, the Transgenic Animal and the Cellular Imaging platforms, University of Lausanne. This work was supported by the Swiss National Foundation (grants FNRS 31003A-127147/1 and 31003A_144198/1 to E. Hummler) and the Swiss National Center of Competence in Research (NCCR Kidney.CH).

Author Contributions

G.C. and S.F. and conducted most of the experiments, including phenotypic characterization of the transgenic lines. S.F. designed constructs and analyzed transgenic mice. J.I. and V.Z.

performed and analyzed the bioinformatic data. L.B., A.M.M., V.N. and C.S. conducted and assisted in *Xenopus* oocytes injection, construct preparation and immunofluorescence experiments. G.C., S.F. and E.H. analyzed the data. S.F. and E.H. wrote the manuscript, conceived, designed and supervised the study.

References

1. Hedstrom, L. (2002) Serine protease mechanism and specificity. *Chemical reviews* **102**, 4501-4524
2. Lopez-Otin, C., and Overall, C. M. (2002) Protease degradomics: a new challenge for proteomics. *Nat Rev Mol Cell Biol* **3**, 509-519
3. Ramachandran, R., Noorbakhsh, F., Defea, K., and Hollenberg, M. D. (2012) Targeting proteinase-activated receptors: therapeutic potential and challenges. *Nature reviews. Drug discovery* **11**, 69-86
4. Magert, H. J., Drogemuller, K., and Raghunath, M. (2005) Serine proteinase inhibitors in the skin: role in homeostasis and disease. *Current protein & peptide science* **6**, 241-254
5. Leyvraz, C., Charles, R. P., Rubera, I., Guitard, M., Rotman, S., Breiden, B., Sandhoff, K., and Hummler, E. (2005) The epidermal barrier function is dependent on the serine protease CAP1/Prss8. *The Journal of cell biology* **170**, 487-496
6. Verghese, G. M., Tong, Z. Y., Bhagwandin, V., and Caughey, G. H. (2004) Mouse prostasin gene structure, promoter analysis, and restricted expression in lung and kidney. *American journal of respiratory cell and molecular biology* **30**, 519-529
7. Adachi, M., Kitamura, K., Miyoshi, T., Narikiyo, T., Iwashita, K., Shiraishi, N., Nonoguchi, H., and Tomita, K. (2001) Activation of epithelial sodium channels by prostasin in Xenopus oocytes. *J Am Soc Nephrol* **12**, 1114-1121
8. Planes, C., Randrianarison, N. H., Charles, R. P., Frateschi, S., Cluzeaud, F., Vuagniaux, G., Soler, P., Clerici, C., Rossier, B. C., and Hummler, E. (2009) ENaC-mediated alveolar fluid clearance and lung fluid balance depend on the channel-activating protease 1. *EMBO molecular medicine* **2**, 26-37
9. Chen, L. M., Skinner, M. L., Kauffman, S. W., Chao, J., Chao, L., Thaler, C. D., and Chai, K. X. (2001) Prostasin is a glycosylphosphatidylinositol-anchored active serine protease. *The Journal of biological chemistry* **276**, 21434-21442
10. Yu, J. X., Chao, L., and Chao, J. (1994) Prostasin is a novel human serine proteinase from seminal fluid. Purification, tissue distribution, and localization in prostate gland. *The Journal of biological chemistry* **269**, 18843-18848
11. Yu, J. X., Chao, L., and Chao, J. (1995) Molecular cloning, tissue-specific expression, and cellular localization of human prostasin mRNA. *The Journal of biological chemistry* **270**, 13483-13489
12. Vallet, V., Chraibi, A., Gaeggeler, H. P., Horisberger, J. D., and Rossier, B. C. (1997) An epithelial serine protease activates the amiloride-sensitive sodium channel. *Nature* **389**, 607-610
13. Vuagniaux, G., Vallet, V., Jaeger, N. F., Hummler, E., and Rossier, B. C. (2002) Synergistic activation of ENaC by three membrane-bound channel-activating serine proteases (mCAP1, mCAP2, and mCAP3) and serum- and glucocorticoid-regulated kinase (Sgk1) in Xenopus Oocytes. *The Journal of general physiology* **120**, 191-201
14. Frateschi, S., Keppner, A., Malsure, S., Iwaszkiewicz, J., Sergi, C., Merillat, A. M., Fowler-Jaeger, N., Randrianarison, N., Planes, C., and Hummler, E. (2012) Mutations of the serine protease CAP1/Prss8 lead to reduced embryonic viability, skin defects, and decreased ENaC activity. *The American journal of pathology* **181**, 605-615
15. Malsure, S., Wang, Q., Charles, R. P., Sergi, C., Perrier, R., Christensen, B. M., Maillard, M., Rossier, B. C., and Hummler, E. (2014) Colon-Specific Deletion of Epithelial Sodium Channel Causes Sodium Loss and Aldosterone Resistance. *J Am Soc Nephrol*

16. Andreasen, D., Vuagniaux, G., Fowler-Jaeger, N., Hummler, E., and Rossier, B. C. (2006) Activation of Epithelial Sodium Channels by Mouse Channel Activating Proteases (mCAP) Expressed in Xenopus Oocytes Requires Catalytic Activity of mCAP3 and mCAP2 but not mCAP1. *J Am Soc Nephrol* **17**, 968-976
17. Frateschi, S., Camerer, E., Crisante, G., Rieser, S., Membrez, M., Charles, R. P., Beermann, F., Stehle, J. C., Breiden, B., Sandhoff, K., Rotman, S., Haftek, M., Wilson, A., Ryser, S., Steinhoff, M., Coughlin, S. R., and Hummler, E. (2011) PAR2 absence completely rescues inflammation and ichthyosis caused by altered CAP1/Prss8 expression in mouse skin. *Nature communications* **2**, 161
18. Chen, L. M., Zhang, X., and Chai, K. X. (2004) Regulation of prostasin expression and function in the prostate. *The Prostate* **59**, 1-12
19. Wakida, N., Kitamura, K., Tuyen, D. G., Maekawa, A., Miyoshi, T., Adachi, M., Shiraishi, N., Ko, T., Ha, V., Nonoguchi, H., and Tomita, K. (2006) Inhibition of prostasin-induced ENaC activities by PN-1 and regulation of PN-1 expression by TGF-beta1 and aldosterone. *Kidney international* **70**, 1432-1438
20. Gettins, P. G. (2002) Serpin structure, mechanism, and function. *Chemical reviews* **102**, 4751-4804
21. Huntington, J. A. (2011) Serpin structure, function and dysfunction. *J Thromb Haemost* **9 Suppl 1**, 26-34
22. Guenther, J., Nick, H., and Monard, D. (1985) A glia-derived neurite-promoting factor with protease inhibitory activity. *The EMBO journal* **4**, 1963-1966
23. Murer, V., Spetz, J. F., Hengst, U., Altrogge, L. M., de Agostini, A., and Monard, D. (2001) Male fertility defects in mice lacking the serine protease inhibitor protease nexin-1. *Proceedings of the National Academy of Sciences of the United States of America* **98**, 3029-3033
24. Jensen, P. J., Yang, T., Yu, D. W., Baker, M. S., Risse, B., Sun, T. T., and Lavker, R. M. (2000) Serpins in the human hair follicle. *J Invest Dermatol* **114**, 917-922
25. Feutz, A.-C., Barrandon, Y., and Monard, D. (2008) Control of thrombin signaling through PI3K is a mechanism underlying plasticity between hair follicle dermal sheath and papilla cells. *Journal of cell science* **121**, 1435-1443
26. Porret, A., Merillat, A. M., Guichard, S., Beermann, F., and Hummler, E. (2006) Tissue-specific transgenic and knockout mice. *Methods in molecular biology (Clifton, N.J* **337**, 185-205
27. Planes, C., Leyvraz, C., Uchida, T., Angelova, M. A., Vuagniaux, G., Hummler, E., Matthay, M., Clerici, C., and Rossier, B. (2005) In vitro and in vivo regulation of transepithelial lung alveolar sodium transport by serine proteases. *Am J Physiol Lung Cell Mol Physiol* **288**, L1099-1109
28. del Vescovo, C. D., Cotecchia, S., and Diviani, D. (2013) A-kinase-anchoring protein-Lbc anchors IkappaB kinase beta to support interleukin-6-mediated cardiomyocyte hypertrophy. *Molecular and cellular biology* **33**, 14-27
29. Geering, K., Theulaz, I., Verrey, F., Hauptle, M. T., and Rossier, B. C. (1989) A role for the beta-subunit in the expression of functional Na+-K+-ATPase in Xenopus oocytes. *The American journal of physiology* **257**, C851-858
30. Wilm, M., Shevchenko, A., Houthaeve, T., Breit, S., Schweigerer, L., Fotsis, T., and Mann, M. (1996) Femtomole sequencing of proteins from polyacrylamide gels by nano-electrospray mass spectrometry. *Nature* **379**, 466-469
31. Shevchenko, A., Wilm, M., Vorm, O., and Mann, M. (1996) Mass spectrometric sequencing of proteins silver-stained polyacrylamide gels. *Analytical chemistry* **68**, 850-858

32. Keller, A., Nesvizhskii, A. I., Kolker, E., and Aebersold, R. (2002) Empirical statistical model to estimate the accuracy of peptide identifications made by MS/MS and database search. *Analytical chemistry* **74**, 5383-5392
33. Nesvizhskii, A. I., Keller, A., Kolker, E., and Aebersold, R. (2003) A statistical model for identifying proteins by tandem mass spectrometry. *Analytical chemistry* **75**, 4646-4658
34. Rickert, K. W., Kelley, P., Byrne, N. J., Diehl, R. E., Hall, D. L., Montalvo, A. M., Reid, J. C., Shipman, J. M., Thomas, B. W., Munshi, S. K., Darke, P. L., and Su, H. P. (2008) Structure of human prostasin, a target for the regulation of hypertension. *The Journal of biological chemistry* **283**, 34864-34872
35. Stout, T. J., Graham, H., Buckley, D. I., and Matthews, D. J. (2000) Structures of active and latent PAI-1: a possible stabilizing role for chloride ions. *Biochemistry* **39**, 8460-8469
36. Li, W., and Huntington, J. A. (2012) Crystal structures of protease nexin-1 in complex with heparin and thrombin suggest a 2-step recognition mechanism. *Blood* **120**, 459-467
37. Sali, A., and Blundell, T. L. (1993) Comparative protein modelling by satisfaction of spatial restraints. *J Mol Biol* **234**, 779-815
38. Melo, F., and Feytmans, E. (1997) Novel knowledge-based mean force potential at atomic level. *J Mol Biol* **267**, 207-222
39. de Vries, S. J., van Dijk, A. D., and Bonvin, A. M. (2006) WHISCY: what information does surface conservation yield? Application to data-driven docking. *Proteins* **63**, 479-489
40. Chen, R., Li, L., and Weng, Z. (2003) ZDOCK: an initial-stage protein-docking algorithm. *Proteins* **52**, 80-87
41. de Vries, S. J., van Dijk, M., and Bonvin, A. M. (2010) The HADDOCK web server for data-driven biomolecular docking. *Nature protocols* **5**, 883-897
42. Berendsen, H. J. C., van der Spoel, D., and van Drunen, R. (1995) GROMACS: A message-passing parallel molecular dynamics implementation. *Computer Physics Communications* **91**, 43-56
43. MacKerell, A. D., Bashford, D., Bellott, Dunbrack, R. L., Evanseck, J. D., Field, M. J., Fischer, S., Gao, J., Guo, H., Ha, S., Joseph-McCarthy, D., Kuchnir, L., Kuczera, K., Lau, F. T. K., Mattos, C., Michnick, S., Ngo, T., Nguyen, D. T., Prodhom, B., Reiher, W. E., Roux, B., Schlenkrich, M., Smith, J. C., Stote, R., Straub, J., Watanabe, M., Wiórkiewicz-Kuczera, J., Yin, D., and Karplus, M. (1998) All-Atom Empirical Potential for Molecular Modeling and Dynamics Studies of Proteins†. *The Journal of Physical Chemistry B* **102**, 3586-3616
44. Gohlke, H., Kiel, C., and Case, D. A. (2003) Insights into protein-protein binding by binding free energy calculation and free energy decomposition for the Ras-Raf and Ras-RalGDS complexes. *J Mol Biol* **330**, 891-913
45. Guerois, R., Nielsen, J. E., and Serrano, L. (2002) Predicting changes in the stability of proteins and protein complexes: a study of more than 1000 mutations. *J Mol Biol* **320**, 369-387
46. Lindner, J. R., Kahn, M. L., Coughlin, S. R., Sambrano, G. R., Schauble, E., Bernstein, D., Foy, D., Hafezi-Moghadam, A., and Ley, K. (2000) Delayed Onset of Inflammation in Protease-Activated Receptor-2-Deficient Mice. *J Immunol* **165**, 6504-6510
47. Hummler, E., Dousse, A., Rieder, A., Stehle, J. C., Rubera, I., Osterheld, M. C., Beermann, F., Frateschi, S., and Charles, R. P. (2013) The channel-activating protease CAP1/Prss8 is required for placental labyrinth maturation. *PloS one* **8**, e55796

48. Chen, M., Fu, Y. Y., Lin, C. Y., Chen, L. M., and Chai, K. X. (2007) Prostasin induces protease-dependent and independent molecular changes in the human prostate carcinoma cell line PC-3. *Biochimica et biophysica acta* **1773**, 1133-1140
49. Friis, S., Uzzun Sales, K., Godiksen, S., Peters, D. E., Lin, C. Y., Vogel, L. K., and Bugge, T. H. (2013) A matriptase-prostasin reciprocal zymogen activation complex with unique features: prostasin as a non-enzymatic co-factor for matriptase activation. *The Journal of biological chemistry* **288**, 19028-19039
50. Peters, D. E., Szabo, R., Friis, S., Shylo, N. A., Sales, K. U., Holmbeck, K., and Bugge, T. H. (2014) The Membrane-Anchored Serine Protease Prostasin (CAP1/PRSS8) Supports Epidermal Development and Postnatal Homeostasis Independent of its Enzymatic Activity. *The Journal of biological chemistry*
51. Camerer, E., Barker, A., Duong, D. N., Ganesan, R., Kataoka, H., Cornelissen, I., Darragh, M. R., Hussain, A., Zheng, Y. W., Srinivasan, Y., Brown, C., Xu, S. M., Regard, J. B., Lin, C. Y., Craik, C. S., Kirchhofer, D., and Coughlin, S. R. (2010) Local protease signaling contributes to neural tube closure in the mouse embryo. *Developmental cell* **18**, 25-38
52. Netzel-Arnett, S., Currie, B. M., Szabo, R., Lin, C.-Y., Chen, L.-M., Chai, K. X., Antalis, T. M., Bugge, T. H., and List, K. (2006) Evidence for a Matriptase-Prostasin Proteolytic Cascade Regulating Terminal Epidermal Differentiation. *J. Biol. Chem.* **281**, 32941-32945
53. Ying, S., O'Connor, B., Ratoff, J., Meng, Q., Mallett, K., Cousins, D., Robinson, D., Zhang, G., Zhao, J., Lee, T. H., and Corrigan, C. (2005) Thymic stromal lymphopoietin expression is increased in asthmatic airways and correlates with expression of Th2-attracting chemokines and disease severity. *J Immunol* **174**, 8183-8190
54. Koyama, K., Ozawa, T., Hatsushika, K., Ando, T., Takano, S., Wako, M., Suenaga, F., Ohnuma, Y., Ohba, T., Katoh, R., Sugiyama, H., Hamada, Y., Ogawa, H., Okumura, K., and Nakao, A. (2007) A possible role for TSLP in inflammatory arthritis. *Biochemical and biophysical research communications* **357**, 99-104
55. Ebner, S., Nguyen, V. A., Forstner, M., Wang, Y. H., Wolfram, D., Liu, Y. J., and Romani, N. (2007) Thymic stromal lymphopoietin converts human epidermal Langerhans cells into antigen-presenting cells that induce proallergic T cells. *The Journal of allergy and clinical immunology* **119**, 982-990
56. Soumelis, V., and Liu, Y. J. (2004) Human thymic stromal lymphopoietin: a novel epithelial cell-derived cytokine and a potential key player in the induction of allergic inflammation. *Springer seminars in immunopathology* **25**, 325-333
57. Soumelis, V., Reche, P. A., Kanzler, H., Yuan, W., Edward, G., Homey, B., Gilliet, M., Ho, S., Antonenko, S., Lauerma, A., Smith, K., Gorman, D., Zurawski, S., Abrams, J., Menon, S., McClanahan, T., de Waal-Malefyt Rd, R., Bazan, F., Kastelein, R. A., and Liu, Y. J. (2002) Human epithelial cells trigger dendritic cell mediated allergic inflammation by producing TSLP. *Nat Immunol* **3**, 673-680
58. Briot, A., Deraison, C., Lacroix, M., Bonnart, C., Robin, A., Besson, C., Dubus, P., and Hovnanian, A. (2009) Kallikrein 5 induces atopic dermatitis-like lesions through PAR2-mediated thymic stromal lymphopoietin expression in Netherton syndrome. *The Journal of experimental medicine* **206**, 1135-1147
59. Wilson, S. R., The, L., Batia, L. M., Beattie, K., Katibah, G. E., McClain, S. P., Pellegrino, M., Estandian, D. M., and Bautista, D. M. (2013) The Epithelial Cell-Derived Atopic Dermatitis Cytokine TSLP Activates Neurons to Induce Itch. *Cell* **155**, 285-295

60. List, K., Szabo, R., Molinolo, A., Sriuranpong, V., Redeye, V., Murdock, T., Burke, B., Nielsen, B. S., Gutkind, J. S., and Bugge, T. H. (2005) Deregulated matriptase causes ras-independent multistage carcinogenesis and promotes ras-mediated malignant transformation. *Genes & development* **19**, 1934-1950
61. Herz, J., and Strickland, D. K. (2001) LRP: a multifunctional scavenger and signaling receptor. *The Journal of clinical investigation* **108**, 779-784
62. Knauer, M. F., Hawley, S. B., and Knauer, D. J. (1997) Identification of a binding site in protease nexin I (PN1) required for the receptor mediated internalization of PN1-thrombin complexes. *The Journal of biological chemistry* **272**, 12261-12264
63. Fayard, B., Bianchi, F., Dey, J., Moreno, E., Djaffer, S., Hynes, N. E., and Monard, D. (2009) The serine protease inhibitor protease nexin-1 controls mammary cancer metastasis through LRP-1-mediated MMP-9 expression. *Cancer research* **69**, 5690-5698
64. Huntington, J. A., Read, R. J., and Carrell, R. W. (2000) Structure of a serpin-protease complex shows inhibition by deformation. *Nature* **407**, 923-926
65. Tully, D. C., Vidal, A., Chatterjee, A. K., Williams, J. A., Roberts, M. J., Petrassi, H. M., Spraggon, G., Bursulaya, B., Pacoma, R., Shipway, A., Schumacher, A. M., Danahay, H., and Harris, J. L. (2008) Discovery of inhibitors of the channel-activating protease prostasin (CAP1/PRSS8) utilizing structure-based design. *Bioorganic & medicinal chemistry letters* **18**, 5895-5899

Figure legends

Figure 1: K14-CAP1/Prss8^{HDS-A} ectopic expression results in hyperkeratosis, inflammation and itch

(A) Representations of the K14-CAP1/Prss8 (upper panel) and K14-CAP1/Prss8^{HDS-A} (lower panel) constructs containing the mouse CAP1/Prss8 coding sequences (wild-type and HDS-A mutant, respectively), the human K14 promoter, the rabbit β-globin intron and the human growth hormone polyadenylation signal (polyA). Restriction sites used for isolation of the transgene (*Cla*I, *Not*I) and for Southern blot analysis (*Eco*RV and *Xba*I) are indicated. For transgene-specific genotyping, primers 1 and 2, and for reverse transcriptase (RT)-PCR, primers 3 and 4 (arrows) were used. **(B)** Total (endogenous gene plus transgene, left panel), transgenic (middle panel) and endogenous *CAP1/Prss8* mRNA expression in the skin determined by quantitative RT-PCR analysis and normalized to β-actin. n ≥3 per genotype. **(C)** Immunofluorescence (green) shows transgenic CAP1/Prss8 expression in the basal layer of the epidermis in *K14-CAP1/Prss8^{HDS-A}* transgenic mice. Nuclei were counterstained with DAPI (blue). The white bar indicates 20 μm, n ≥ 3 mice/genotype. Objective Plan-Apochromat 63x/1.4 Oil, magnification 630x, pinhole 96 μm. **(D)** Macroscopic appearance of *K14-CAP1/Prss8*, *K14-CAP1/Prss8^{HDS-A}* transgenic mice and control (wild-type) littermates at 2 weeks of age (upper panels) and corresponding haematoxylin and eosin analyses (lower panels). Scale bar indicates 20 μm; n = 3 mice per genotype. (**E**) Epidermal differentiation markers (keratin-14, -6, -1, filaggrin, loricrin and involucrin) as present (green) in both wild-type and transgenic mice. Dotted lines indicate basal membrane. Nuclei are counterstained with DAPI (blue). Scale bar represents 20 μm, objective Plan-Apochromat 63x/1.4 Oil, magnification 630x, pinhole 96 μm; n = 3 mice per group. (**F**) Transepidermal water loss (TEWL) measurements of the indicated genotypes. n ≥ 6 animals per group. (**G**) Quantitative RT-PCR examination of *TSLP, MMP9, IL-1α* and *IL-1β* in wild-type and transgenic skin

normalized to *β-actin*. (**H**) Dot plot indicating the duration of the scratching behavior expressed in percentage, n=5 per group. Bars indicate the average of the time spent scratching.

Figure 2 PAR2 interacts with CAP1/Prss8 wild-type and CAP1/Prss8^{HDS-A} *in vitro*

(A) Representative Western blot resulting from HEK-293 cells co-transfected with wild-type or CAP1/Prss8^{HDS-A} Flag-tagged, and PAR2 or $\alpha_1\beta_2$ adrenergic receptor HA-tagged. Cell lysates were immunoprecipitated with anti-HA and analyzed using anti-HA and anti-Flag antibodies. The $\alpha_1\beta_2$ adrenergic receptor was used as negative control. **(B)** Representative Western blot resulting from HEK-293 cells co-transfected with wild-type or CAP1/Prss8^{HDS-A} Flag-tagged, and PAR2 or $\alpha_1\beta_2$ adrenergic receptor HA-tagged. Cell lysates were immunoprecipitated with anti-Flag and analyzed using anti-Flag and anti-HA antibodies. The $\alpha_1\beta_2$ adrenergic receptor was used as negative control. Results are representative of three independent experiments.

Figure 3 Ichthyosis and inflammation are absent in *K14-CAP1/Prss8^{HDS-A}; PAR2 -/-* mice

(A) Total CAP1/Prss8 (endogenous gene plus *K14-CAP1/Prss8^{HDS-A}* transgene) expression in the skin determined by quantitative RT-PCR analysis and normalized to β-actin; n ≥ 8 per genotype. **(B)** *PAR2* expression in the skin determined by quantitative RT-PCR analysis and normalized to *β-actin*; n ≥ 4 per genotype. **(C)** Macroscopic appearance of 2-week-old animals (upper panels) and corresponding haematoxylin and eosin staining of skin (lower panels). n ≥ 3 mice per group. Bar represents 20 μm. **(D)** Measurement of epidermal thickness of the indicated genotypes expressed in μm; n ≥ 3 animals per genotype. **(E)** TEWL analyses in experimental and control animals; n ≥ 8 mice per group. **(F)** Quantitative RT-PCR examination of *TSLP, MMP-9, Il-1α* and *IL-1β* in experimental and control animals

normalized to β-actin; n ≥ 3 per genotype. (**G**) Dot plot indicating the duration of the scratching behavior expressed in percentage. Bars indicate the average of the time spent scratching; n ≥ 3 per genotype.

Figure 4 CAP1/Prss8 and nexin-1 interact *in vitro* despite CAP1/Prss8^{HDS-A} mutations

(A) Representative Western blots resulting from HEK-293 cells co-transfected with CAP1/Prss8 wild-type or CAP1/Prss8^{HDS-A} Flag-tagged and nexin-1. Cell lysates were immunoprecipitated with anti-Flag and analyzed using anti-Flag and anti-nexin-1 antibodies. The Flag tag was used as negative control. Results are representative of three independent experiments. **(B)** Amiloride-sensitive sodium currents expressed in μA from three independent experiments pulled together, each consisting of at least five *Xenopus* oocytes measured per condition. **(C)** Homology model of mouse CAP1/Prss8 and nexin-1 tertiary protein structure. The residues of the serine protease active site, Asp 134, His 85, and Ser 238 (HDS), are represented in violet and the amino acids of the reactive center loop of nexin-1 are colored in yellow. The figure shows the best orientation of the two molecules when bound to form a stable complex, as resulted from docking analyses using ZDOCK and HADDOCK programs. **(D)** Zoomed view showing the predicted interacting regions of CAP1/Prss8 and nexin-1. CAP1/Prss8 residues involved in the interaction are represented in light blue, and nexin-1 residues in green. **(E)** Representative Western blots resulting from HEK-293 cells co-transfected with wild-type (wt) or E247A (E-A) CAP1/Prss8 Flag-tagged and with nexin-1. Cell lysates were immunoprecipitated with anti-Flag and analyzed using anti-Flag and anti-nexin-1 antibodies. The Flag tag was used as negative control. Results are representative of three independent experiments.

Figure 5 *K14-nexin-1* transgenic mice do not present any obvious skin defects

(A) Scheme of the K14-nexin-1 construct containing the mouse *nexin-1* coding sequence (cDNA, g.i. 229093415), the human *K14* promoter, the rabbit *β-globin* intron and the human growth hormone polyadenylation signal (polyA). Restriction sites used for isolation of the transgene (*Xba*I) and for Southern blot analysis (*Bam*HI and *Eco*RV) are indicated. For transgene-specific genotyping, primers 1 and 2 (arrows) were used. **(B)** Total *nexin-1* (endogenous gene plus transgene) mRNA expression in the skin determined by quantitative RT-PCR analysis and normalized to *β-actin*; n ≥3 per genotype. **(C)** Representative Western blot analysis of total nexin-1 (endogenous gene plus transgene) protein expression in the skin. β-actin was used as loading control; n ≥3 per genotype. **(D)** Macroscopic appearance of *K14-nexin-1* transgenic mice and control littermates at 2 weeks of age (upper panels) and corresponding haematoxylin and eosin analyses (lower panels). Scale bar indicates 20 μm; *n* = 3 mice per genotype. **(E)** TEWL analyses in experimental and control animals; n ≥ 8 mice per group.

Figure 6 Ichthyosis and increased water loss are strongly attenuated in *K14-CAP1/Prss8; K14-nexin-1* and *K14-CAP1/Prss8^{HDS-A}; K14-nexin-1* double transgenic mice

(A) Total *CAP1/Prss8* (endogenous gene plus transgene) mRNA expression in the skin determined by quantitative RT-PCR analysis and normalized to *β-actin* in *K14-CAP1/Prss8; K14-nexin-1* and *K14-CAP1/Prss8^{HDS-A}; K14-nexin-1* animals; n ≥3 per genotype. **(B)** Total *nexin-1* (endogenous gene plus transgene) mRNA expression in the skin determined by quantitative RT-PCR analysis and normalized to *β-actin* in *K14-CAP1/Prss8; K14-nexin-1* and *K14-CAP1/Prss8^{HDS-A}; K14-nexin-1* animals; n ≥ 3 per genotype. **(C)** Macroscopic appearance of the indicated genotypes at 2 weeks of age (upper panels) and corresponding haematoxylin and eosin analyses of the skin (lower panels). Scale bar indicates 20 μm; n ≥ 3

mice per genotype. **(D)** Measurement of epidermal thickness of the indicated genotypes expressed in µm; n ≥ 3 animals per genotype. **(E)** Body weight measurements of 2-week-old male transgenic mice and littermate controls. **(F)** TEWL analyses in single and double *K14-CAP1/Prss8; K14-nexin-1* transgenic mice and wild-type controls; n ≥ 8 mice per group. **(G)** TEWL analyses in single and double *K14-CAP1/Prss8^{HDS-A}; K14-nexin-1* transgenic mice and wild-type controls; n ≥ 8 mice per group.

Figure 7 Inflammation is prevented in *K14-CAP1/Prss8; K14-nexin-1* and *K14-CAP1/Prss8^{HDS-A}; K14-nexin-1* double transgenic mice

(A) Quantitative RT-PCR examination of *TSLP, MMP-9, Il-1α* and *IL-1β* in experimental and control *K14-CAP1/Prss8; K14-nexin-1* animals normalized to *β-actin*; n ≥ 3 per genotype. **(B)** Quantitative RT-PCR examination of *TSLP, MMP-9, Il-1α* and *IL-1β* in experimental and control *K14-CAP1/Prss8^{HDS-A}; K14-nexin-1* animals normalized to *β-actin*; n ≥ 3 per genotype.

Table 1. The three *K14-CAP1/Prss8*$^{HDS-A}$ founders resulted in three independent transgenic lines.

Genotype **Breeding pairs**	**wild-type**	***K14-CAP1/Prss8***$^{HDS-A}$
F$_0$1, *K14-CAP1/Prss8*$^{HDS-A}$ x WT, *n=195*	114	81
Observed, %	(58.5)	(41.5)
Expected, %	(50)	(50)
χ 2	ns	ns
scaly skin phenotype	no	yes, 61 (75) no, 20 (25)
F$_0$2, *K14-CAP1/Prss8*$^{HDS-A}$ x WT, *n=108*	60	48
Observed, %	(55.6)	(44.4)
Expected, %	(50)	(50)
χ 2	ns	ns
scaly skin phenotype	no	yes, 16 (33) no, 32 (67)
F$_0$3, *K14-CAP1/Prss8*$^{HDS-A}$ x WT, *n=100*	67	33
Observed, %	(67)	(33)
Expected, %	(50)	(50)
χ 2	p<0.01	p<0.01
scaly skin phenotype	no	no

Pronuclear injections yielded three *K14-CAP1/Prss8*$^{HDS-A}$ founders that resulted in three independent transgenic lines (F$_0$1, F$_0$2 and F$_0$3). Pups were analyzed during the first 3 weeks after birth. Number of mice for recorded genotype is indicated. Percentages are reported in brackets. ns: non-significant. Data reported in the manuscript derived from animals originated from the first founder (F$_0$1).

Table 2. PAR2 deficiency prevents the *K14-CAP1/Prss8^{HDS-A}*-induced phenotype in double *K14-CAP1/Prss8^{HDS-A};PAR2 -/-* mice.

Genotype	***K14-CAP1/Prss8^{HDS-A}***		***K14-CAP1/Prss8^{HDS-A}***		***K14-CAP1/Prss8^{HDS-A}***	
Breeding pairs	***PAR2 -/-***	***PAR2 -/-***	***PAR2 +/-***	***PAR2 +/-***	***PAR2 +/+***	***PAR2 +/+***
K14-CAP1/Prss8^{HDS-A};PAR2 +/-	18	20	41	26	19	20
x *PAR2 +/-, n=131*						
Observed %	(12.5)	(13.9)	(28.5)	(18)	(13.2)	(13.9)
Expected %	(12.5)	(12.5)	(25)	(25)	(12.5)	(12.5)
X^2	ns	ns	ns	ns	ns	ns
scaly skin phenotype	no	no	yes, 23 (56)	no	yes, 18 (95)	no
			no, 18 (44)		no, 1 (5)	

Pups were analyzed during the first 3 weeks after birth. Number of mice for recorded genotype is indicated**.** Percentages are reported in brackets. ns: non-significant.

Table 3. Co-expression of nexin-1 alleviates the CAP1/Prss8 and the CAP1/Prss8^{HDS-A}-induced phenotype.

Genotype **Breeding pairs**	**WT**	***K14-CAP1/Prss8***	***K14-nexin-1***	***K14-CAP1/Prss8*** ***K14-nexin-1***
K14-CAP1/Prss8 line1 X *K14-nexin-1*, n=182	46	37	47	52
Observed %	(25)	(20)	(26)	(29)
Expected %	(25)	(25)	(25)	(25)
X^2	ns	ns	ns	ns
scaly skin phenotype	no	yes	no	yes, 2 (4) no, 50 (96)
K14-CAP1/Prss8 line2 X *K14-nexin-1*, n=151	37	26	43	45
Observed %	(24.5)	(17.2)	(28.5)	(29.8)
Expected %	(25)	(25)	(25)	(25)
X^2	ns	ns	ns	ns
scaly skin phenotype	no	yes	no	yes, 16 (36) no, 29 (64)
K14-CAP1/Prss8^{HDS-A} X *K14-nexin-1*, n=109	38	33	20	18
Observed %	(34.9)	(30.3)	(18.3)	(16.5)
Expected %	(25)	(25)	(25)	(25)
X^2	ns	ns	ns	ns
scaly skin phenotype	no	yes, 24 (73) no, 9 (27)	no	yes, 2 (11) no, 16 (89)

Pups were analyzed during the first 3 weeks after birth. Number of mice for recorded genotype is indicated. Percentages are reported in brackets. ns: non-significant.

Figure 1

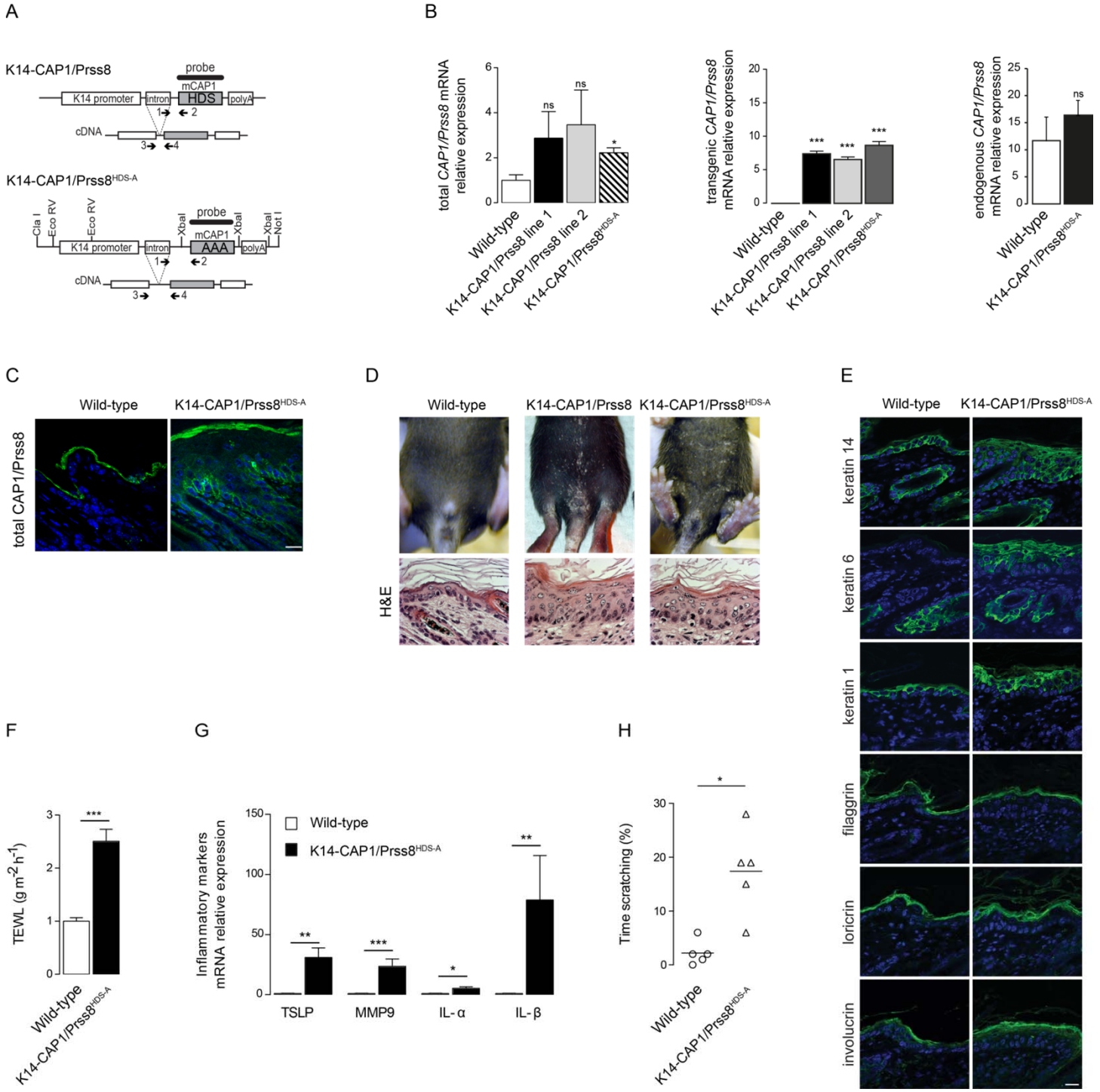
A
K14-CAP1/Prss8
probe
mCAP1
K14 promoter
intron
HDS
polyA
cDNA
K14-CAP1/Prss8HDS-A
Cla I
Eco RV
Eco RV
XbaI
probe
XbaI
XbaI
Not I
AAA
B
total CAP1/Prss8 mRNA relative expression
transgenic CAP1/Prss8 mRNA relative expression
endogenous CAP1/Prss8 mRNA relative expression
ns
***
*
Wild-type
K14-CAP1/Prss8 line 1
K14-CAP1/Prss8 line 2
K14-CAP1/Prss8HDS-A
C
Wild-type
K14-CAP1/Prss8HDS-A
total CAP1/Prss8
D
Wild-type
K14-CAP1/Prss8
K14-CAP1/Prss8HDS-A
H&E
E
Wild-type
K14-CAP1/Prss8HDS-A
keratin 14
keratin 6
keratin 1
filaggrin
loricrin
involucrin
F
TEWL (g m-2 h-1)
G
Inflammatory markers mRNA relative expression
Wild-type
K14-CAP1/Prss8HDS-A
TSLP
MMP9
IL-α
IL-β
H
Time scratching (%)

Figure 2

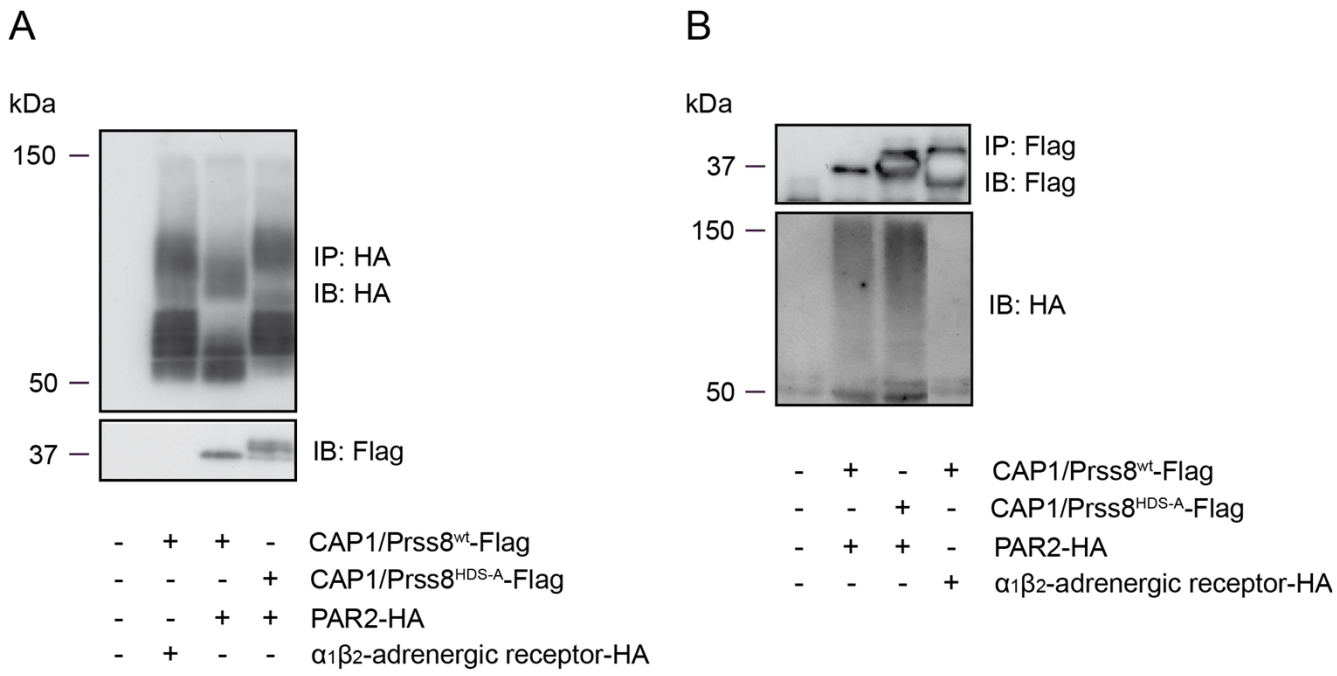
A
kDa
150
50
37
IP: HA
IB: HA
IB: Flag
- + + - CAP1/Prss8wt-Flag
- - - + CAP1/Prss8HDS-A-Flag
- - + + PAR2-HA
- + - - α1β2-adrenergic receptor-HA
B
kDa
37
150
50
IP: Flag
IB: Flag
IB: HA
- + - + CAP1/Prss8wt-Flag
- - + - CAP1/Prss8HDS-A-Flag
- + + - PAR2-HA
- - - + α1β2-adrenergic receptor-HA

Figure 3

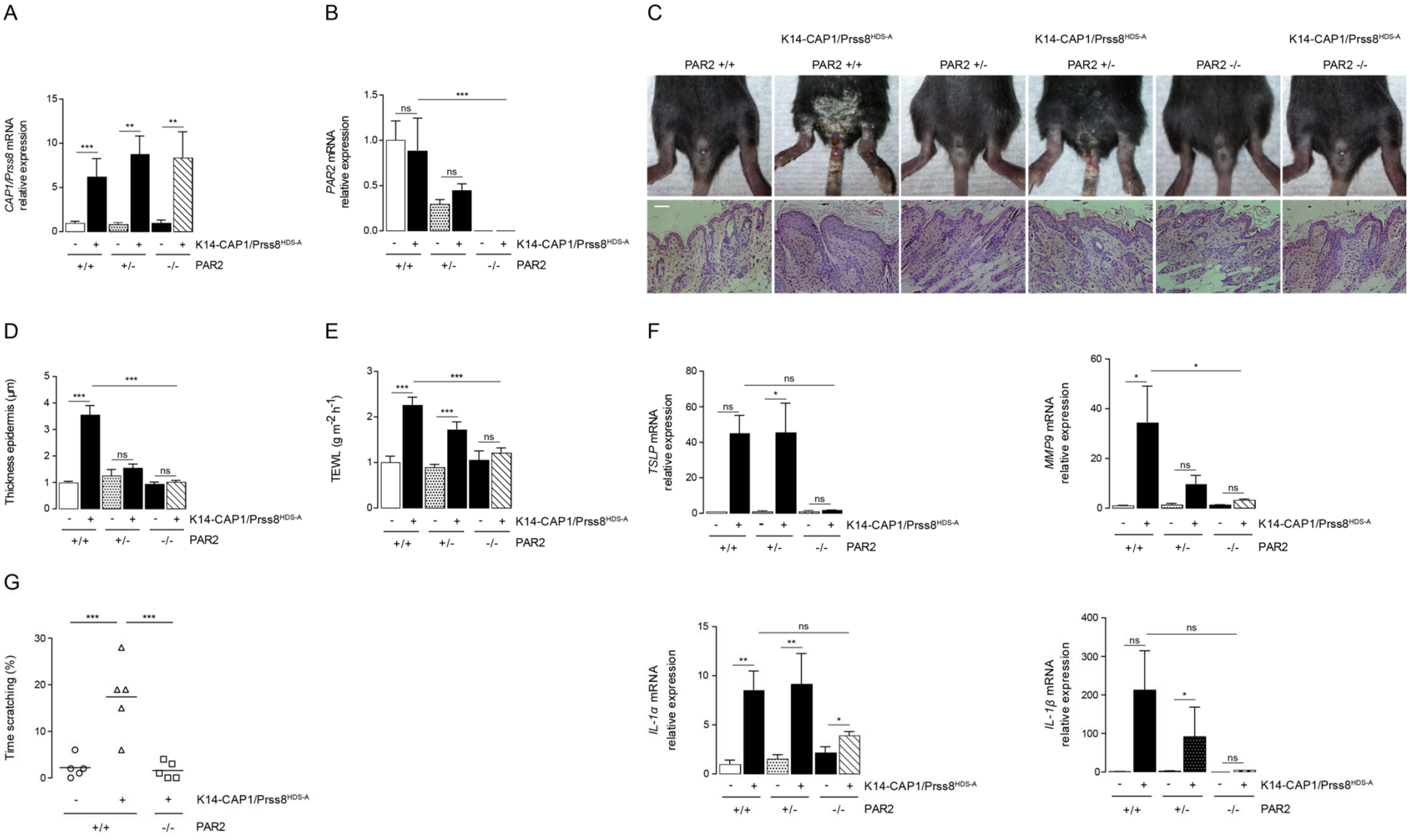
A
CAP1/Prss8 mRNA relative expression
K14-CAP1/Prss8HDS-A
PAR2
+/+
+/-
-/-
B
PAR2 mRNA relative expression
C
K14-CAP1/Prss8HDS-A
PAR2 +/+
PAR2 +/-
PAR2 -/-
D
Thickness epidermis (µm)
E
TEWL (g m-2 h-1)
F
TSLP mRNA relative expression
MMP9 mRNA relative expression
IL-1α mRNA relative expression
IL-1β mRNA relative expression
G
Time scratching (%)

Figure 4

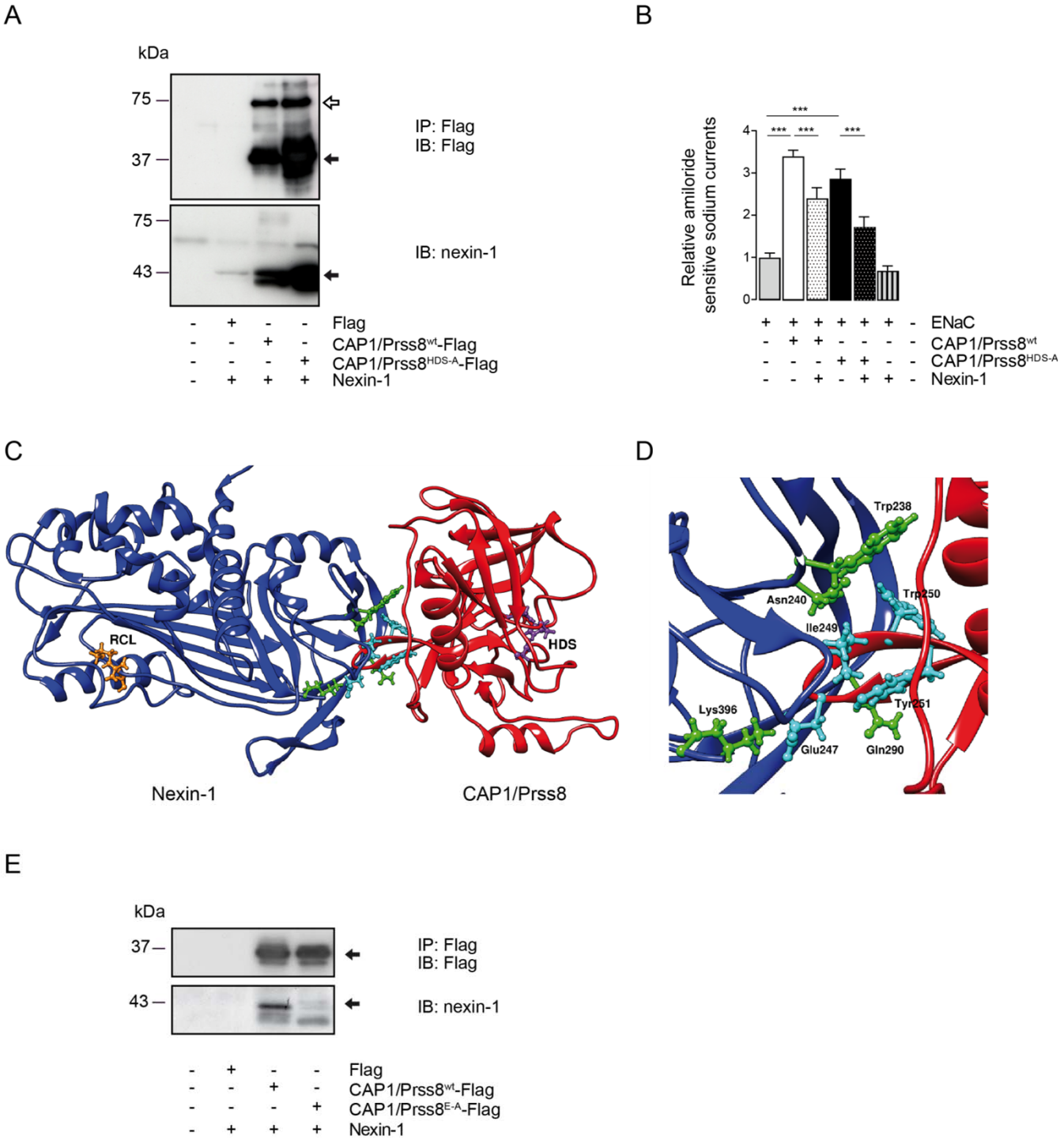
A
kDa
75
37
75
43
IP: Flag
IB: Flag
IB: nexin-1
- + - - Flag
- - + - CAP1/Prss8wt-Flag
- - - + CAP1/Prss8HDS-A-Flag
- + + + Nexin-1
B
Relative amiloride sensitive sodium currents
0
1
2
3
4
***
***
***
***
+ + + + + + - ENaC
- + + - - - - CAP1/Prss8wt
- - - + + - - CAP1/Prss8HDS-A
- - + - + + - Nexin-1
C
RCL
HDS
Nexin-1
CAP1/Prss8
D
Trp238
Asn240
Trp250
Ile249
Lys396
Tyr251
Glu247
Gln290
E
kDa
37
43
IP: Flag
IB: Flag
IB: nexin-1
- + - - Flag
- - + - CAP1/Prss8wt-Flag
- - - + CAP1/Prss8E-A-Flag
- + + + Nexin-1

Figure 5

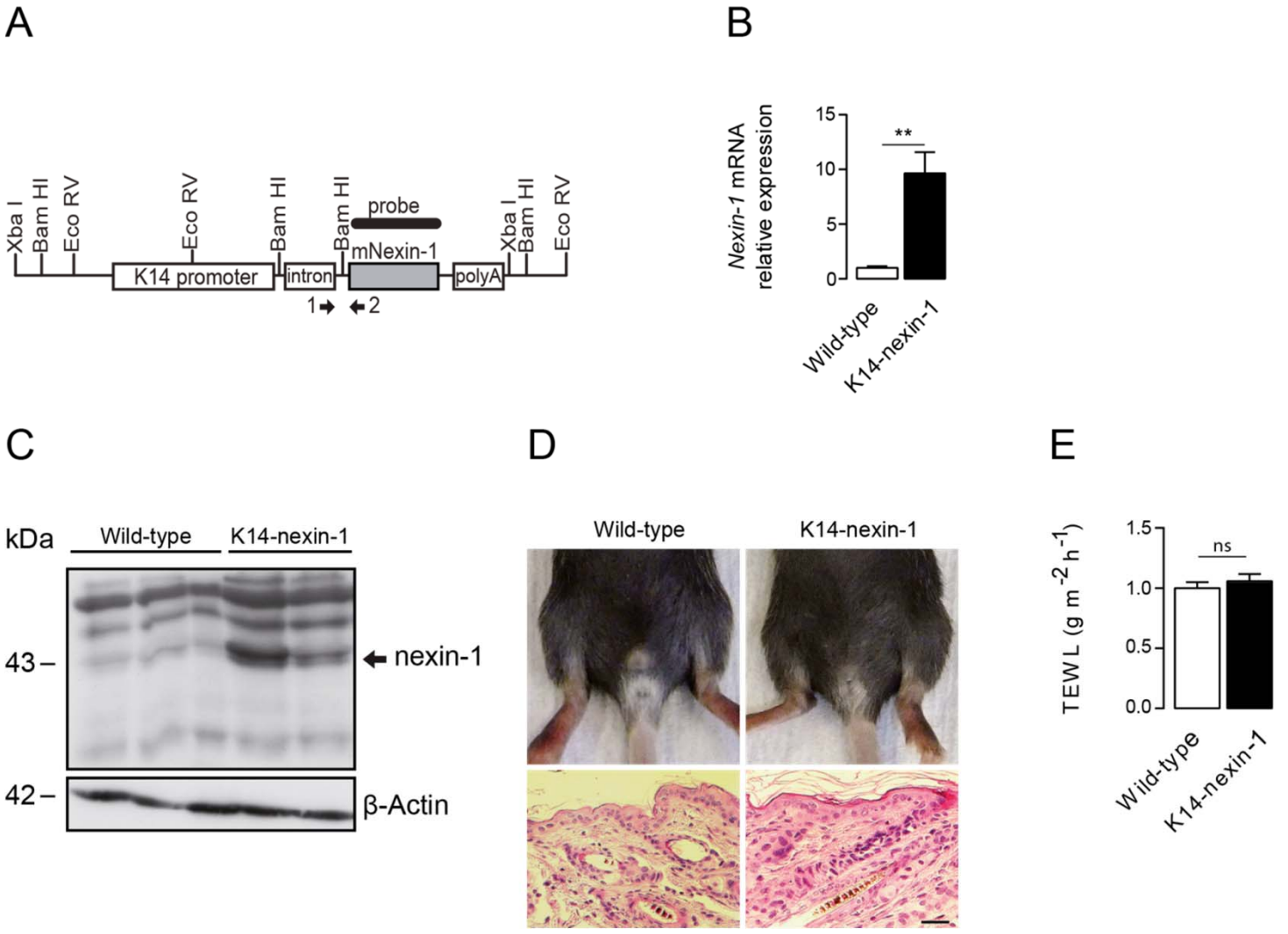
A
Xba I
Bam HI
Eco RV
Eco RV
Bam HI
Bam HI
probe
mNexin-1
Xba I
Bam HI
Eco RV
K14 promoter
intron
polyA
1
2
B
Nexin-1 mRNA relative expression
15
10
5
0
**
Wild-type
K14-nexin-1
C
kDa
Wild-type
K14-nexin-1
43 –
nexin-1
42 –
β-Actin
D
Wild-type
K14-nexin-1
E
TEWL (g m-2 h-1)
1.5
1.0
0.5
0.0
ns
Wild-type
K14-nexin-1

Figure 6

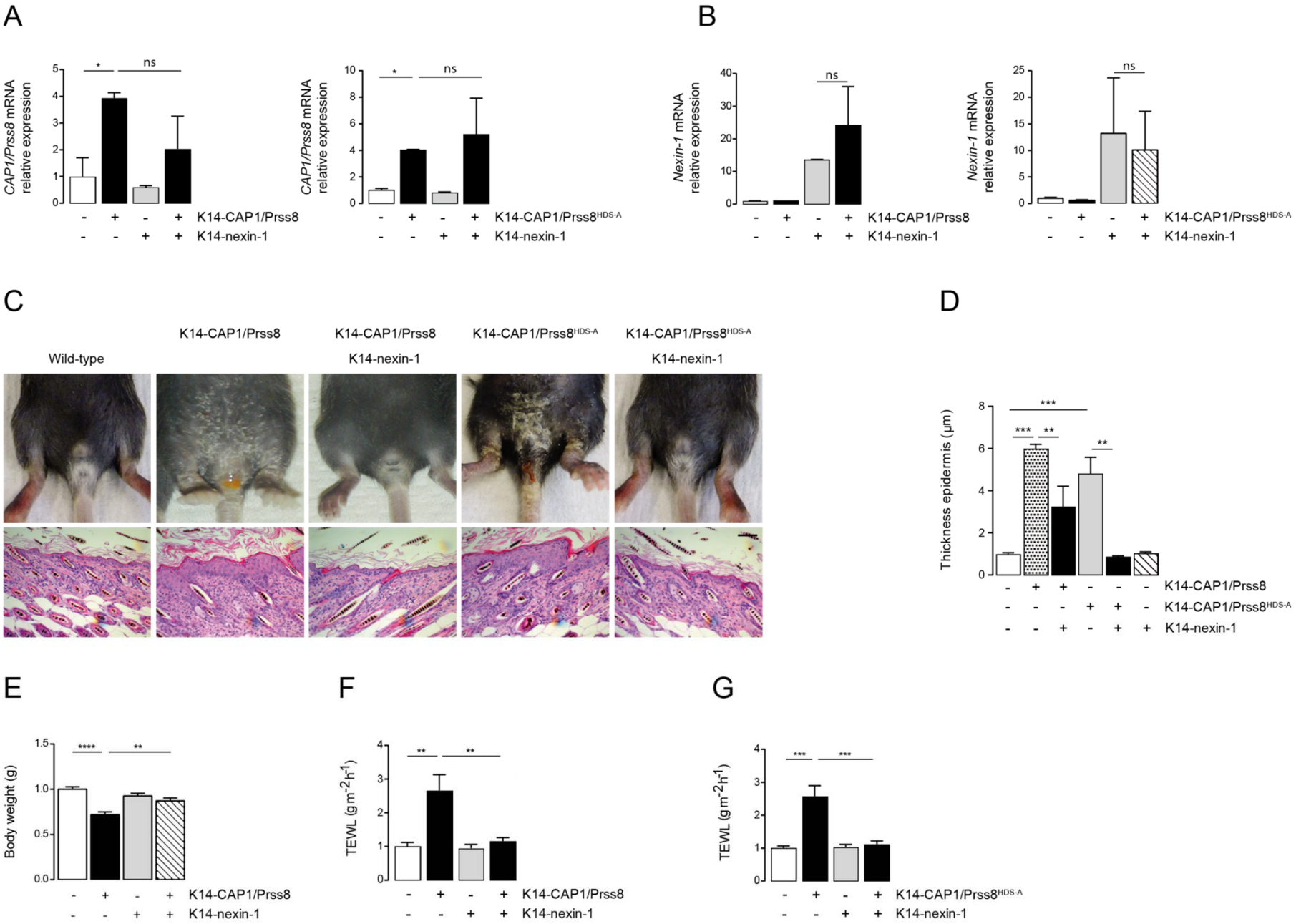
A
CAP1/Prss8 mRNA relative expression
*
ns
K14-CAP1/Prss8
K14-nexin-1
CAP1/Prss8 mRNA relative expression
K14-CAP1/Prss8HDS-A
K14-nexin-1
B
Nexin-1 mRNA relative expression
ns
K14-CAP1/Prss8
K14-nexin-1
Nexin-1 mRNA relative expression
K14-CAP1/Prss8HDS-A
K14-nexin-1
C
Wild-type
K14-CAP1/Prss8
K14-CAP1/Prss8
K14-nexin-1
K14-CAP1/Prss8HDS-A
K14-CAP1/Prss8HDS-A
K14-nexin-1
D
Thickness epidermis (µm)
***
**
K14-CAP1/Prss8
K14-CAP1/Prss8HDS-A
K14-nexin-1
E
Body weight (g)
****
**
K14-CAP1/Prss8
K14-nexin-1
F
TEWL (g m-2h-1)
**
K14-CAP1/Prss8
K14-nexin-1
G
TEWL (g m-2h-1)
***
K14-CAP1/Prss8HDS-A
K14-nexin-1

Figure 7

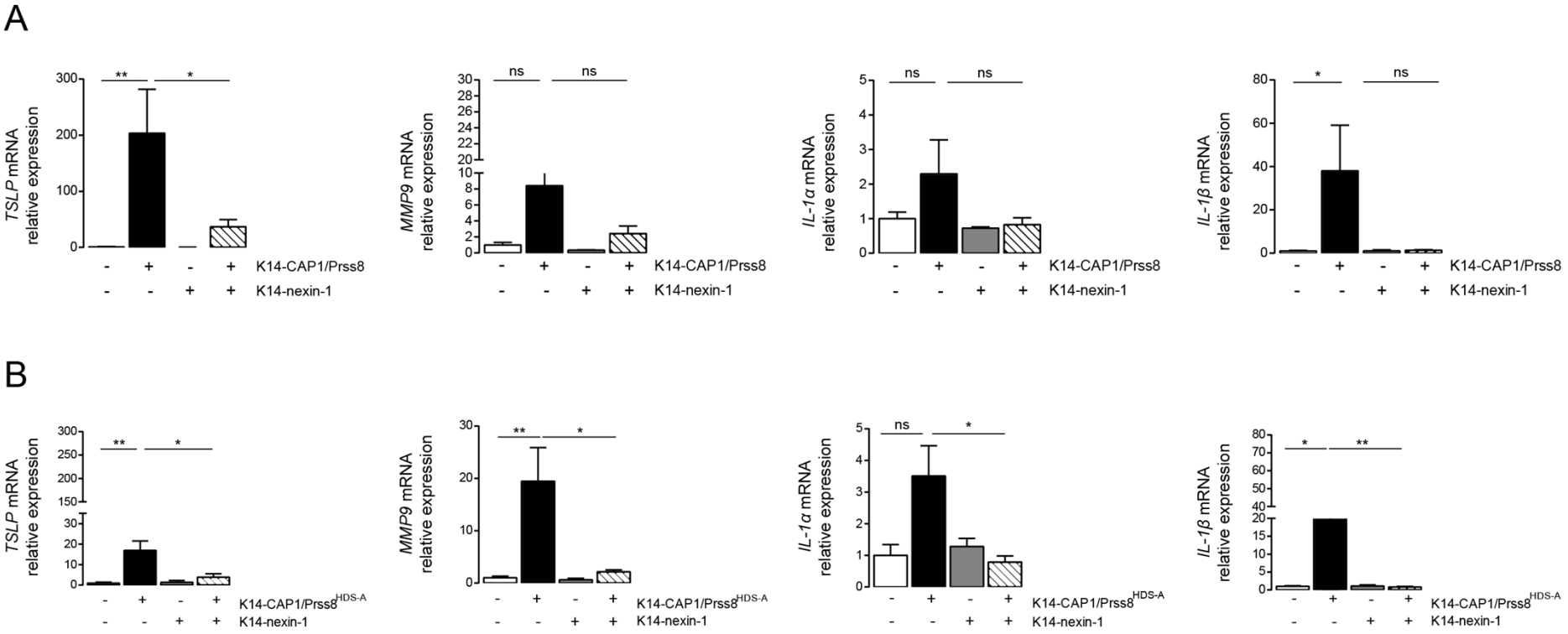
A
TSLP mRNA relative expression
MMP9 mRNA relative expression
IL-1α mRNA relative expression
IL-1β mRNA relative expression
K14-CAP1/Prss8
K14-nexin-1
B
TSLP mRNA relative expression
MMP9 mRNA relative expression
IL-1α mRNA relative expression
IL-1β mRNA relative expression
K14-CAP1/Prss8HDS-A
K14-nexin-1